Master Degree project

Pilot Study for Data-driven Modification of Face Specific Material Properties

Master Degree Project in Virtual Product Realization
Two year Level 30 ECTS
Spring term 2025

Manfred Persson

Supervisor: Rohollah Ghasemi

Examiner: Kent Salomonsson

Abstract

This pilot study is meant to start off a larger current larger project at the University of Skövde. In the larger study synergy research between lasers, compacted graphite iron, and photodiode in situ monitoring are to be studies. Through the use of lasers, the surface of the compacted graphite iron is to be heat treated for wear resistance and strength. The photodiode will create data to be used for simulation and neural networks to evaluate optimal process parameters. As such, this pilot study engages in making initial discoveries from which further research in the larger project can be based. To do so a scheme of action research is adopted, where iterations of plan-act-reflect drives the project forward. Through five iterations two main methods are tried and their results documented. The study shows that it is possible to create a hardened surface layer using lasers. It also gives some indication on how to continue work in the larger project, to possibly create a material with favourable material parameters from a single irradiation.

Keywords: Compacted Graphite Iron, Heat Treatment, Photodiode, Data Retrieval, Heat Imager, Laser Hardening.

UNIVERSITY
OF SKÖVDE

Acknowledgements

This project would not have been possible without the help of some companies with departments and employees located in Skövde. Those were Martina Axen and Anders Ericsson at Volvo Trucks, Lars Tööj at IDC West Sweden AB, and Goran Ljustina and Peter Eriksson at Aurobay Technologies. I would also like to thank my supervisor Rohollah Ghasemi, my examiner Kent Salomonsson, and my colleagues at Skövde University.

And lastly I would like to give special recognition and thanks to Tage Persson who once again have offered unyielding strength and support throughout the tribulations of my academic endeavours.

Skövde, June 2025

Manfred Persson

Certificate of Authenticity

Submitted by Manfred Persson to the University of Skövde as a Master's Degree Thesis at the School of Engineering.

I certify that all material in this Master Thesis Project which is not my own work has been properly referenced.

Manfred Persson

Certification
and
Declaration on the Use of Artificial Intelligence (AI) Tools during the degree project

This report has been submitted by Manfred Persson to the University of Skövde as a requirement for the degree of Master of Science in Computational Methods in Engineering.

The undersigned certifies that all the material in this report that is not my own has been properly acknowledged using accepted referencing practices and, further, that the report includes no material for which I have previously received academic credit.

As part of my commitment to academic integrity and transparency, I hereby declare the extent to which I have used Artificial Intelligence (AI) tools during the preparation and writing of this report. This declaration does not apply to the use of basic tools for checking grammar, spelling, references etc.

Please check all that apply:

☐ **No use of AI tools**
I have not used any AI-based tools or services in any part of the research, writing, analysis, or presentation of this report.

☐ **Language editing assistance only**
I have used AI tools exclusively for language correction, grammar checking, or stylistic improvements. No substantive content was generated or modified by AI.

☐ **Idea generation / brainstorming**
I used AI tools to help generate initial ideas, brainstorm possible research questions, or explore conceptual frameworks. The final work and conclusions are my own.

☐ **Methodology design**
I used AI tools to assist in designing the research methodology (e.g., structuring experiments, surveys, or models). The methodology has been critically reviewed and adapted by me.

☑ **Programming or code assistance**
I used AI-based coding assistants to help write or debug code. All code has been reviewed, tested, and modified by me.

☐ **Data analysis / processing support**
I used AI tools to assist with data analysis, visualization, or statistical processing. Interpretations and conclusions were drawn independently.

☐ **Content generation (text, figures, tables)**
AI tools were used to generate portions of text, diagrams, or tables that appear in this report. Such content has been critically reviewed, fact-checked, and appropriately cited where applicable.

☑ **Other (please specify):**
I was given access to Scopus AI which I used when searching for papers with specific themes.

Responsibility Statement
I confirm that all AI-assisted contributions have been used ethically and in accordance with institutional guidelines. I take full responsibility for the accuracy, originality, and academic integrity of the content presented in this report.

I understand that any misuse or misrepresentation of AI tool usage may be considered a breach of academic conduct and could result in disciplinary actions, including revocation of the report and/or the academic degree awarded.

Signature:

Name: Manfred Persson

Date: 23/6-25

UNIVERSITY OF SKÖVDE

Table of Contents

Abstract **2**

Acknowledgements **3**

Certificate of Authenticity **4**

Certification and Declaration on the Use of Artificial Intelligence (AI) Tools during the degree project **5**

Table of Contents **8**

Table of Figures **10**

Index of Tables **11**

1 Introduction **12**
1.1 Research Approach . . . 12
1.2 Scope and limitations . . . 12

2 Theoretical framework **14**
2.1 Laser Welder and Laser Beam Modulation . . . 14
2.2 Hardening and Rapid Hardening in CGIs . . . 17
2.3 Data Collection . . . 19
2.3.1 Temperature measurements with thermocouples . . . 19
2.3.2 Temperature measurements with thermal Imaging and emissivity . . . 20
2.3.3 Photodiode sensor . . . 20
2.3.4 Vicker's hardness . . . 21

3 Method **22**
3.1 Iteration 1 - Plan . . . 22
3.2 Iteration 1 - Act . . . 23
3.3 Iteration 2 - Plan . . . 25
3.4 Iteration 2 - Act . . . 25
3.5 Iteration 3 - Plan . . . 26
3.6 Iteration 3 - Act . . . 27
3.7 Iteration 4 - Plan . . . 27
3.8 Iteration 4 - Act . . . 28
3.9 Iteration 5 - Plan . . . 29
3.10 Iteration 5 - Act . . . 31

3.11 Analysis of Iteration 4 and 5 Data . . . 32
3.11.1 Hardness Testing och Microscopy . . . 32
3.11.2 Data handling with MATLAB . . . 32
3.11.3 Heat Map Construction . . . 33

4 Results **34**
4.1 Iteration 1 - Reflection . . . 34
4.2 Iteration 2 - Reflection . . . 35
4.3 Iteration 3 - Reflection . . . 36
4.4 Iteration 4 - Reflection . . . 36
4.5 Iteration 5 - Reflection . . . 41

5 Discussion **47**

6 Conclusions **48**
6.1 iteration 4 . . . 48
6.2 iteration 5 . . . 48

7 Future work **49**

References **52**

8 Appedix **53**

UNIVERSITY OF SKÖVDE

Table of Figures

1 Simplified Schematic of Laser Fibre. . . . 14
2 Intensity of CF and RF with various modulations. . . . 15
3 Simplified Schematic of the Trumpf Laser Machine. . . . 15
4 Laser modulation with Gaussian density spread diagrams. . . . 16
5 Hardening diagram of irons based of their various carbon contents. . . . 17
6 Graphite morphology of compacted graphite iron. . . . 17
7 Microstructure of as-cast and austenised compacted graphite iron. . . . 17
8 Simplified schematic of thermocouple setup. . . . 19
9 Simplified schematic of experimental setup containing a thermal imager and a photodiode sensor. . . . 20
10 Diagram over the five iterations included in this paper. . . . 22
11 Cutting machine, Discotom-100 from Struers. . . . 23
12 Grinding and polishing machine, Tegramin-30 from Struers. . . . 23
13 Experimental setup of iteration 1 through 4. . . . 24
14 Power modulation over time for test 42. . . . 25
15 Power modulation in 3 step variations. . . . 26
16 Power modulation with 3 variations. . . . 28
17 Thermal image showing max temp and temp profiles horizontally and vertically aligned with max temp. . . . 29
18 Test sample 96 cut along the documented horizontal temperature profile. . . . 29
19 Experimental setup for iteration 5. . . . 31
20 Distances with which the two laser machine programs irradiate with. . . . 31
21 Assumed location of hardened surface layers in red in cross-sections of iteration 4 (left) and iteration 5 (right). . . . 32
22 Horizontal temperature profiles of tests 100 (above) and 101 (below). . . . 34
23 Power modulation vs. temperature of test 45. . . . 35
24 Power modulation and temperature of test 58c. . . . 36
25 Comparison between test 99 and test 100. . . . 36
26 Microstructure near surface of tests 101 (above), 105 (middle), 97 (below). . . . 37
27 Vickers indent in darker area of test 97. . . . 38
28 Vickers indent in darker area of test 101. . . . 38
29 Images of heat signatures after 30 s, 40 s, 50 s, and 60 s of irradiation. . . . 39
30 Wavelength mean value for data points between 4 second mark and 26 second mark for tests 97, 101, and 105. . . . 40
31 Change in smoothed light emission value by wavelength between 30 s and 60 s for tests 97, 101, and 105. . . . 40

32 Test sample 9a. 41
33 Test sample 9b. 41
34 Cross section from test 9a. 41
35 Images from hardness measurements in iteration 5. 42
36 Wavelength 1017 nm of tests 1b - 9b. 43
37 Peak values in 32 wavelengths for tests with 3 lines. 44
38 Peak values in 32 wavelengths for tests with 5 lines. 44
39 Heatmap for comparing normalised values of parameters and wavelengths. 45
40 Three images showing crack nucleation in the hardened matrix. 46
41 Comparison of photodiode signal by tests in iteration 4. 56
42 Comparison of photodiode signal by wavelength in iteration 4. 57
43 Thermal imager data from the 18 tests in iteration 5. 58
44 Comparison of photodiode signal by tests of 3 lines in iteration 5. 59
45 Comparison of photodiode signal by wavelength of 3 lines in iteration 5. 60
46 Comparison of photodiode signal by tests of 5 lines in iteration 5. 61
47 Comparison of photodiode signal by wavelength of 5 lines in iteration 5. 62
48 Comparison example of photodiode signal by wavelength from third line of 5 lines in iteration 5. 63

UNIVERSITY OF SKÖVDE

Index of Tables

1 Temperature vs. Time DoE 27
2 power vs. speed settings 30
3 Test results including power, speed, melt pool thickness, and hardness. 42
4 Experimental data from iteration 1.1 53
5 Experimental data from iteration 1.2 53
6 Experimental data from iteration 2 54
7 Experimental data from iteration 3 54
8 Experimental data from iteration 4 55

UNIVERSITY OF SKÖVDE

1 Introduction

Heat treatment for elevated material properties is a prominent economic cost in the production of metal parts. Elevated temperatures are maintained in the metal parts for prolonged periods of time. These kinds of heat treatments are applied to modify the material properties of the metal, like hardness, wear resistance, and ductility. Alloys of carbon, iron, and various other elements needs specialised procedures to achieve the required properties. Precision in times, temperature, heating rates, and cool down rates is vital as to secure process repeatability. Usually, several different procedures are required for the same parts. In this project, methods with possibility for lowering energy expenditure of heat treatment of compacted graphite iron (CGI) by using lasers is explored. When lasers irradiate a material the irradiated surface becomes heated locally, and when the laser is turned off the energy disperse into the surrounding material relatively quickly. This feature makes it possible to heat treat very local areas of the surface, thusly preventing any excessive energy expenditure required to treat the whole piece, where much of the heating may be redundant. In some cases, properties of the substrate of a metal may even have more desirable properties as a subsurface material. Such is the case of the CGI handled in this project. The material is used in a case where where only one surface is exposed to prolonged sliding wear damage, making the substrates excellent thermal conductivity ideal to divert heat from the surface. Thusly, the success of this project can help provide a cheaper, cleaner and more sustainable manufacturing process while also improving the function of the metal part. Furthermore, as this project is a part of a larger project, the some function and result variation when using sensors available at Skövde University (HIS) is included.

1.1 Research Approach

As the equipment and material handled in this project are of high novelty, very much so for the synergy between them, an exploratory approach to the study with mixed methods of analysis, i.e. handling both quantitative and qualitative information, through action research [1] is adapted. Action research is particularly suited for this task, as it consists of iterations of research, describing how professional research projects often functions. The central three stages of action research are plan, act, and reflect [ibid.], although sometimes explained using four [2] or five stages [3]. Seeing as the plan-, act-, reflect-stages are included in all three versions, the iterations involved in this study will be described using the three. The approach is chosen with the task at hand in mind, being that of an initial intelligence grab where groundwork for the larger project can be established.

1.2 Scope and limitations

The projects scope is already established to be evaluating the feasibility of using lasers to affect the surface hardness of CGI materials. Because of this, the limitations included in this project are

the same ones present in the current state of the research department of the engineering faculty of the university. Included in that current state is also the availability of labs of close parters of HIS.

UNIVERSITY OF SKÖVDE

2 Theoretical framework

In this section the theoretical framework of the project is discussed. Any papers or other academic material referenced throughout this paper are gathered and found in a fast and circumstantial manner suitable for a master´s thesis. This is done as an alternative to, for example, explore the state of the art with a systematic review or such [4]. A less time consuming review is especially useful when engaging in action research, as new insight may demand fast reviews to grasp new concepts. The planning part of a new iteration would then possibly include new smaller rapid reviews. When conducting a literary review in this manner some precision and coverage of the subject is lost, while the risk of losing credibility increases. Hence, using secure sources where credibility is already established is a useful rule for the faster review styles.

2.1 Laser Welder and Laser Beam Modulation

The Trumpf Yb:YAG laser machine of the HIS laser laboratory has a maximum output power of 6000 watts and operates at a wavelength of 1030nm. As this report will not touch upon actual welding of metals, or any theory on it, e.g. keyhole formation or melt pool dynamics, it will not be mentioned is this section. What will be mentioned, however, is the laser beam modulation (LBM) and other details central to the study.
The laser beam is emitted either through the core fibre (CF) or ring fibre (RF) of the laser fibre cable, or both (Figure 1).

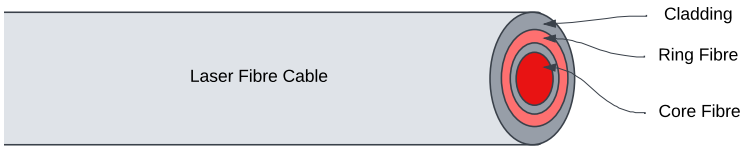

Figure 1: Simplified Schematic of Laser Fibre.

The laser machine used is equipped with a programmable focusing optics (PFO) laser head with which the LBM can be modified. The LBM being the ratio of light emitted with the CF and RF. The modulation ranges from 100 percent in the CF, 0 percent in the RF to 0 percent in the CF, 100 percent in the RF to a total of 100 percent (Figure 2).

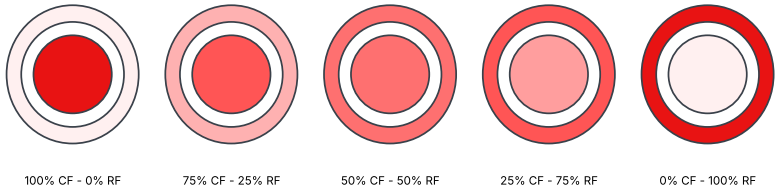

Figure 2: Intensity of CF and RF with various modulations.

The intensity represented by the opacity of the red colour in figure 2 represents a mean value of the actual laser beam. In reality it is emitted with a Gaussian distribution, being more intense towards the middle of the beam. During the welding process, LBM can be used to effect how the weld melt pool is shaped, affecting how the metal solidifies and the resulting material properties [5]. More often then not, such welding is done at a specific length from the optical lens of the welding machine, called the focal length. The laser tilted by the lens which creates, at the focal length distance from the lens, a point where the light is at the maximum irradiance called the focal point (Figure 3). The irradiance of the light is given by $E = P/A$ [6].

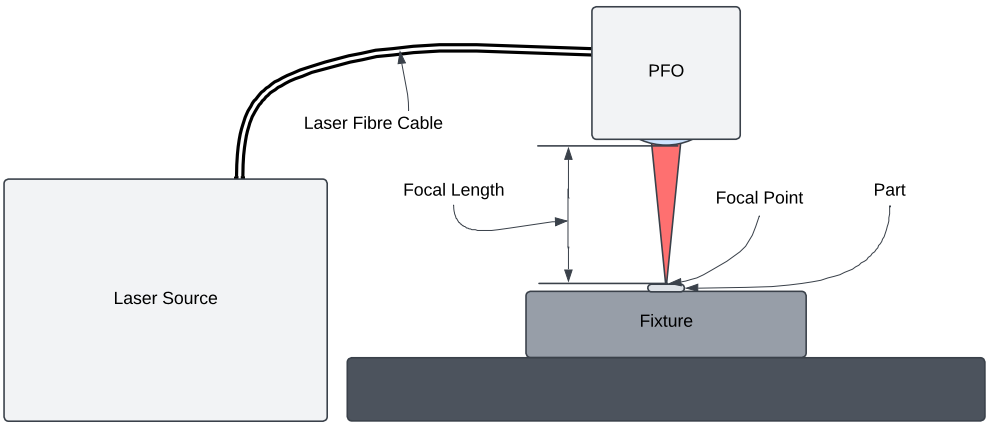

Figure 3: Simplified Schematic of the Trumpf Laser Machine.

The beam is emitted from the optical lens at a 2.7 degrees focusing angle relative the centre of the beam. Meaning that if one was to move the target further from the optical lens than the distance at which the focal point occurs, the area which receives the laser would expand, effectively lowering the irradiance of the beam. Through previous experiments the mean irradiance values available have been confirmed to be between 270 W/m^2 and $6,6 * 10^{10}$ W/m^2. Still, being more concentrated

towards the centre of the area receiving the laser [7]. As seen in figure 4 the CF and RF has its own irradiance spread, albeit the diagrams in the figure are cross-sectional representations of the levels of transferred energy. The modulation of the laser beam becomes an important obstacle in the pilot study, as an irradiance in the lower end of the spectrum is attempted. A beam of lower irradiance should be suitable for controlled and slow heating of the surface of the metal to temperatures useful for hardening [8], specifics of which will be discussed at greater length later.

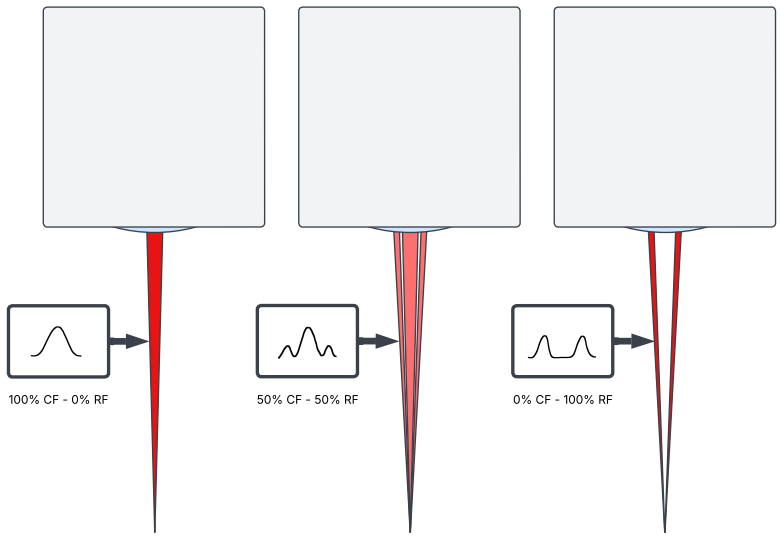

Figure 4: Laser modulation with Gaussian density spread diagrams.

When irradiating a surface it doesn't always absorb the energy at the same rate. Instead, the surface materials roughness and temperature dictate what proportion of the light is absorbed or reflected. The phenomenon of absorption growing with temperature can be assumed in solid metals but not in fluids [9] [10]. Likewise, a rougher surface generally offers more absorption than a smooth surface, since the light can interact more with the rough surface before it is reflected, and thusly transfer more energy to the material [11] [12].

2.2 Hardening and Rapid Hardening in CGIs

For the purposes of this study, induced temperatures between 700°C and 900°C are of interest and this section will thusly be limited to discussing the effects of those temperatures. This is because of austenitisation that happens between these temperatures (and above) (Figure 5) [13] [14]. Austenitisation is a process where the material becomes more uniform as carbon diffuses and carbon from the graphite deposits are dissolved into the matrix [15]. When the material is then cooled down microstructural tensions are created as carbon is trapped in the iron crystalline structure, which raises the materials hardness. How much and in what specific way hardening occurs is one of the more central phenomenons related to material parameters subjected to current and historic research. Why the range have also been of interest in previous related work on hardening of the CGI conducted by HIS researchers. Furthermore the thermal imager available has an upper limit of recognisable temperatures, being 925°C.

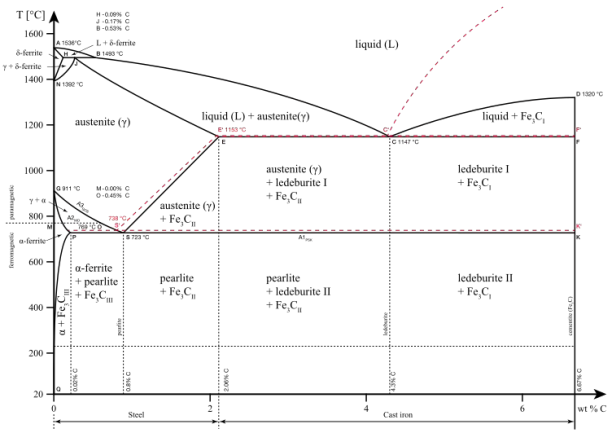

Figure 5: Hardening diagram of irons based of their various carbon contents.

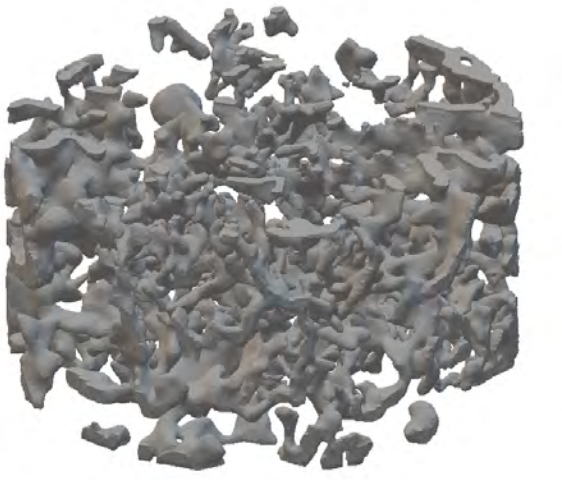

Figure 6: Graphite morphology of compacted graphite iron.

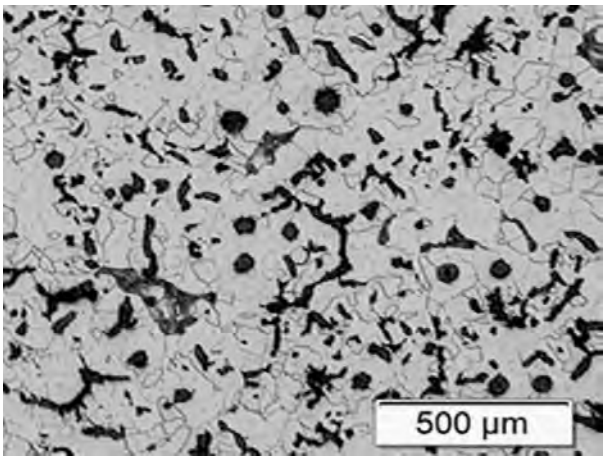

Figure 7: Microstructure of as-cast and austenised compacted graphite iron.

Several different factors affect how steels and cast irons harden, and one factor is the amount of carbon included in the alloy [14]. Other alloying elements may be present which affect hardening. The elements affect is similar to that of carbon and is therefore referred to as their "carbon equivalent" [16]. The material in focus of this study is a ferritic CGI alloyed with around 3,5 percent carbon [17] [18]. A small amount of the alloys carbon is included in the metal matrix but most is contained in the deposits of graphite (figure 6 and 7 [19]). However, the carbon contents was confirmed using an optical emission spectroscopy recognising the metal matrix as well as the graphite deposits.

When the CGI´s internal temperature becomes elevated the graphite diffuses into the metallic matrix [20] raising its carbon content. The temperatures and carbon contents austenitisation happens at can be derived from figure 5. The diffusion process is time dependant and materials are often kept at elevated temperatures for anywhere between 30 minutes to several hours to achieve the wanted effect [21]. For this project such periods of elevated temperatures are not feasible. Instead, rapid heat treatment of a local surface is of interest. The process includes rapidly heating the surface to the desired temperature by applying the laser heat source, then removing it to let the quenching happen. This limits the period which the CGI is exposed to the heat source to seconds, simultaneously limiting the prolonged carbon diffusion. Rapid hardening of CGI's may thusly behave more like that of low carbon steels and may still become hardened without the prolonged diffusion of graphite, albeit to a more limited extent [22] [23]. As the diffusion is left out, graphite morphology may also remain largely intact throughout the heat treated volume [24]. Diffusion of graphite, at the interesting temperature range, into the material would otherwise turn the material into a homogenous alloy, reducing the thermal conductivity of the alloy [25] [26] [24]. If the graphite is allowed to diffuse for a long enough time period it can leave voids in the material causing some decreased material properties [20]. Furthermore, the graphite deposits are sources for crack nucleation [27].

As previously mentioned, when the material has been kept at the elevated austenitisation temperature its temperature is lowered. The lowering of the temperature is called quenching and the speed at which it happens effects the resulting hardness of the material. Generally, higher cool down rates result in higher hardness in grey irons and steels [22] [28]. This is, as briefly mentioned before, because migrating carbon atoms is trapped in irregular places in the material matrix at a higher rate. The trapped carbon in turn causes microstructural strain in the material, which raises the material hardness [28]. The microstructure with trapped carbon is called martensite and is favourable for high hardness, and can be identified through microscopy [29] [19].

2.3 Data Collection

In this project there are four main setups of data acquisition systems (DAQ) that are used for monitoring and analysing the methods used. Temperature measurements are conducted using two different sets of sensors: thermocouples and a thermal imager. The aforementioned photodiode sensor is used to measure process light emission. To evaluate the processes the Vicker's hardness of the materials is tested. In this section the four methods for collecting data are briefly described.

2.3.1 Temperature measurements with thermocouples

Thermocouples are a set of wires that, in this case, are welded to the location where temperature is to be measured. Alternative ways to welding is by screw joint or clamp, however, welding of the wires offers measurements comparatively more suited to capture very local temperatures.

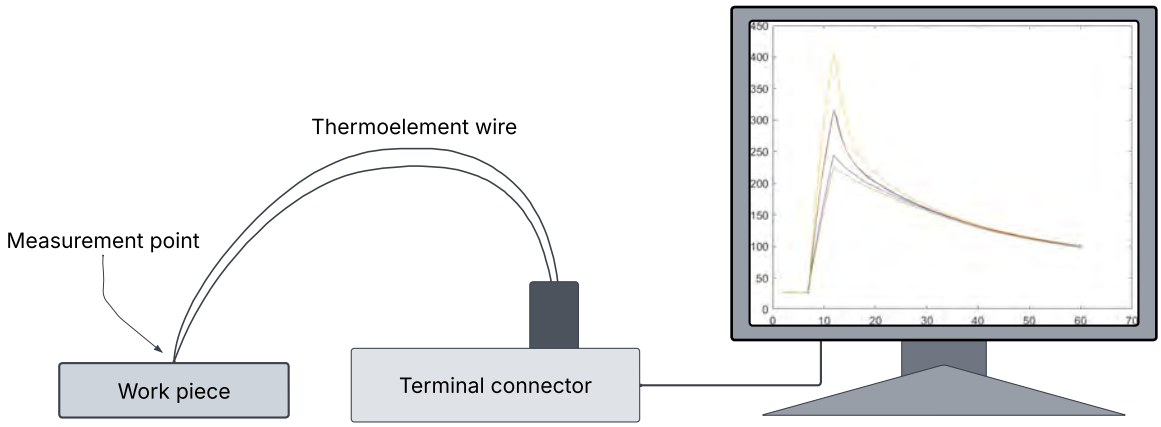

Figure 8: Simplified schematic of thermocouple setup.

The setup used for measuring the temperature with thermocouples can be seen in figure 8. It consist of a two cefir-20-KK ceramic coated wires welded to the location of interest. The wires are connected to a cDAQ-9174 DAQ chassis equipped with a TB-9214 temperature input module, converting the readings of differences in electromotive force [30] to a data stream. The data stream is then fed into a computer where a MATLAB script is used to control the procedure and save the incoming data.

2.3.2 Temperature measurements with thermal Imaging and emissivity

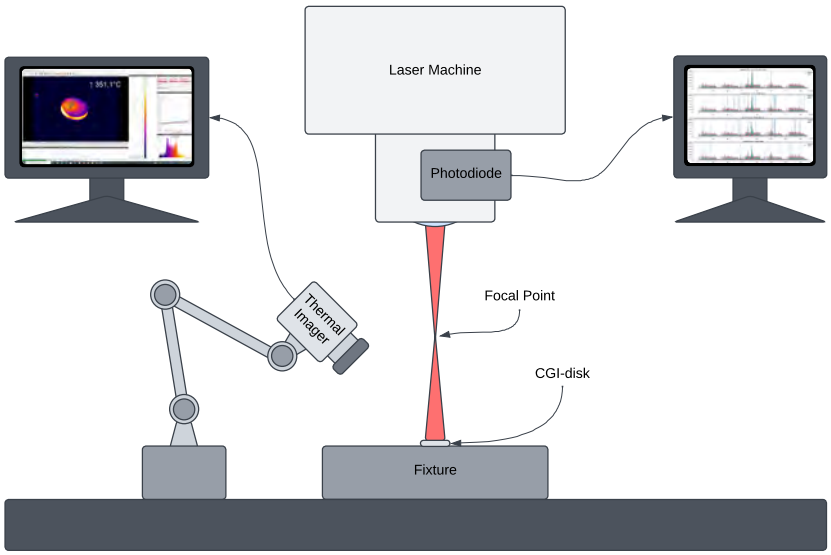

Figure 9: Simplified schematic of experimental setup containing a thermal imager and a photodiode sensor.

Figure 9 depicts how the thermal imager was set up during experiments. The setup consists of a thermoIMAGER TIM 160S connected directly to a computer where the interface TIMConnect is used to operate it. It is documented to be able to measure temperatures between $-20°C$ and $900°C$, even if experiments show that it measures up to $925°C$. It has an uncooled "focal plane array" (FPA) detector that recognises thermal radiation through multiple sensors and converts them into an image with 2% accuracy above $100°C$ [31]. The detector translates the data by a preset emissivity constant purposefully chosen to match that of the material emitting the thermal radiation. The emissivity constant ranges from 0 to 1 where polished mirror-like surfaces has an emissivity closer to 0 and oxidised and darker surfaces are closer to 1. Thusly, events like oxidation of metals which generally accelerates at higher temperatures may change the emissivity of a material while taking measurements.

2.3.3 Photodiode sensor

Figure 9 also includes the simplified schematic of the photodiode sensor. It is a patented 4D.TWO sensor from 4D PHOTONICS GmbH which can detects wavelength magnitudes in 32 wavelength ranges between $300nm$ and $1900nm$. The sensor retrieves the detectable light emissions through the laser optics and filters them around the wavelength that the laser operates at ($1030nm$). A computer then receives the signal through a interface that is specialised for the sensor which also

saves the data in database-files. 16 wavelength ranges are in the visual spectrum and are thusly denoted as "VIS" while the remaining ranges are in the near infrared spectrum and are denoted as "NIR". Each range samples the light emissions at around $6000Hz$ max, but the sampling rate can be lowered for higher resolution. The light emissions that are measured varies in magnitude depending on a number of factors, like changes in element matrix [32], matrix phase changes [33], temperatures changes, or key hole depth flux.

2.3.4 Vicker's hardness

Vicker's hardness is one of the more common kinds of hardness testing. It tests the hardness of a material by pressing a pyramid shaped tool into the material with a given force, and depending on how wide the indent becomes, the Vicker's hardness is derived. The machine use in this project is a QNESS 60 A+ EVO with the capability to measure indents in the micro scale. Therefore, it is possible to measure hardness in individual grains of the microstructure. The machine is operated with a computer with a specialised interface saving data on each individual test sample in pdf and/or image files.

UNIVERSITY OF SKÖVDE

3 Method

In this section the first two action research steps, plan and act, performed in this pilot study is handled. The third step, reflect, is handled in the results section. Five iterations of action research is performed in succession. Throughout the five iterations the focus is to develop a method for how the laser machine could be used for heat treatment to CGI material. Included in the work is testing and applying of various tools and equipment that are suitable for the task at hand (Figure 10).

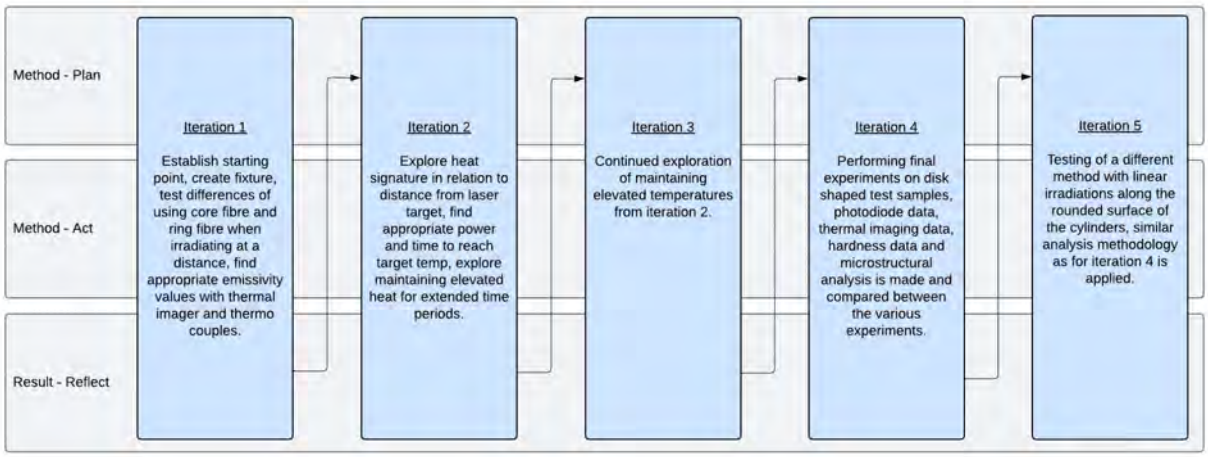

Figure 10: Diagram over the five iterations included in this paper.

After the five subsections handling the five iteration, a sixth subsection handles analysis of data.

3.1 Iteration 1 - Plan

The primary goal of the first step is to measure the emissivity of the CGI material and to explore heat propagation at a further distance from the laser optics relative the focal length. As stated earlier this is important for further usage of the thermal camera available for the project. Measurements of a materials emissivity can be done by measuring the temperature with some other method and adjusting the emissivity setting of the thermal imager to match the real measured temperature. When it does, the real emissivity of the material can be extracted and used in further testing. To retrieve the reference temperature thermocouples are used.
To be able to conduct a large amount of trial runs in the laser machine cutting of the material is considered. This is necessary as the shape and amount of available CGI material inflicts a boundary conditions on the project. The available material consists of around 40 cylinders 60mm in length and with a radius of 15mm is decided to be cut into disks of 2mm thickness. Furthermore, the

material is to be machined so that the surfaces that will receive the laser beam have a uniform surface roughness. Before samples are irradiated they are cleaned in two phases, the first one with gasoline to remove any grease or grime, and the second with acetone to remove any trace from the first cleaning fluid. A simple fixture should be produced to make the setup for each experiment uniform. With these components of the first step of the first iteration planned, the act step can commence.

3.2 Iteration 1 - Act

Figure 11: Cutting machine, Discotom-100 from Struers.

Figure 12: Grinding and polishing machine, Tegramin-30 from Struers.

Starting out with the cutting and grinding of the cylinders using the equipment in the material lab of HIS. The equipment used in this iteration is a Discotom-100 cutting machine and a Tergamin-30 grinding and polishing machine from Struers, and an older manual grinding machine. The cylinders are first manually grinded in the older grinding machine to remove any pre-existing variation in diameters in the cylinder. Each cylinder is then cut in half into two equal sized smaller cylinders to fit in the grinding machine. One side of the smaller cylinder is grinded with 220 grit sandpaper to a specific surface roughness, to then be cut into a 2 mm disk with one grinded side and one raw ungrinded side. This process of grinding one side and then cutting the disk is repeated until the cylinder is too short work continue working with. The process is necessary to be able to achieve the grinded side as 2 mm is well below the minimum thickness a workpiece must have to be grinded in the Tergamin-30. Cutting the disks of 2 mm is done with some difficulty where exact measurements

are hard to pinpoint. Measurements ranges from 1,5 mm to 3 mm and some lopsidedness is present in some of the disks. When approximately 40 disks are available the cutting and grinding phase of the first iteration is concluded and work continues in the laser lab.
Work in the laser lab starts out with assembling the various thermocouples, thermal cameras and other tools needed. The fixture that is to be used is created using a CNC-machine to mill a 1 mm deep circular slot with the same radius as the cylinders. No apparatus to hold down the disks or the like is used as the top surface should be bare to receive the laser beam. Instead, a snug room temperature fit is created. When the disk is heated by the laser it expands, minimising the fit further and preventing movement of the disk. Initially a single disk is placed in the slot to test some variables. The variables being tested are the appropriate power, appropriate power modulation and some durations of applied laser. An appropriate distance between the laser optics was calculated to let the width of the laser beam align with the width of the disk.

To retrieve temperature data five thermocouples are welded to the disk at equal spacings of 3 mm along the radius starting in the centre. As they are welded to the top surface receiving the laser, the thermocouples are located closer to the laser optics than the disk (Figure 3)(Figure 13). Since the disk is placed further from the laser optics than the focal length, the irradiance applied to the disk is lower than the that one applied to the thermocouples. To avoid reading the potentially higher temperature induced in the thermocouples rather than the temperature at the disk surface, half of the disk is covered with a steel plate. The edge of the steel plate is aligned with the radius where the thermocouples are located. Twenty experiments of various combinations of variables (Table 4) the were performed on the same disk.

Figure 13: Experimental setup of iteration 1 through 4.

Moving on from the first single disk variable experiments of iteration 1, with the new information learned. The second experiment is focused on finding the emissivity of the CGI, and as the surface quality of the disk is effected by the heat, emissivity would change as well. As such, eleven tests are performed in succession, each on individual disks. In an attempt to not let the cables of the thermocouple be placed at the spot receiving the maximum irradiance of the laser beam they are welded 5 mm from the middle of the disk. The thermal imager is placed at an around 45 degree

angle to the disk and at a 200 mm distance from it. This is the complete setup for the second experiment of the first iteration. Throughout the experiment laser beam modulation, duration of applied laser and distance from laser optics remain constant, variations of power intensity and emissivity values are changed throughout the experiment (Table 5).

3.3 Iteration 2 - Plan

Having decided what emissivity settings to use for the thermal camera, from this iteration on the thermocouples are omitted. Further testing of the distance to the laser optics are planned. They should show if warming the disk with a larger area receiving the Gaussian laser beam produces a more even heat signature. The experiments in this iteration should also attempt to find settings for power and laser emission time to reach a specific temperature. Furthermore, experiments should explore the possibility of maintaining a specific elevated temperature for a prolonged time. The experiments are performed using only the RF and an emissivity of 0,3.

3.4 Iteration 2 - Act

Experiments of iteration 2 are performed on 13 disks. Starting out variations of power and laser emission time are tested and temperature gain per second of the surface is used for determining the success. As stated earlier, CGI is prone to cracking if exposed to too hasty and large temperature variations. Based on this fact, a slower temperature gradient is desirable. Following duration and temperature experiments distance and laser power modulation is tested. Another instance of laser emission is added to the laser program to attempt the maintenance of prolonged temperature. When adding an instance of laser emission in the laser program it will still act on the same base power, however, there is a possibility to choose what percentage of the power and duration of the instance. As seen in table 6, for example, for test 42, duration and power modulation for the first and second instances are 10 seconds at 50 percent and 5 seconds at 25 percent, respectively. This indicates that for the first 10 seconds the power is at 50 percent of 2000 Watts, i.e. 1000 Watts. For the following 5 seconds, however, the power goes down gradually from 50 percent to 25 percent with a 5 percent decrease per second as seen in figure 14.

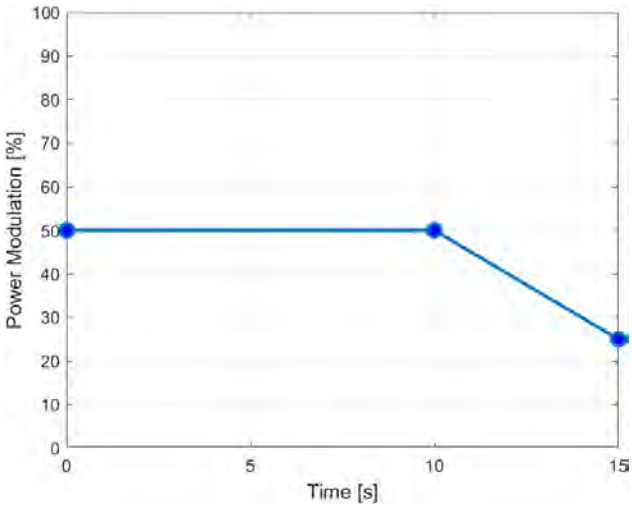

Figure 14: Power modulation over time for test 42.

UNIVERSITY OF SKÖVDE

3.5 Iteration 3 - Plan

For the third iteration the exploration of the power modulations effect on developed heat over time that is touched upon in iteration 2 is continued. The goal is to find some useful setting to keep elevated temperatures constant for extended periods, which will henceforth be called ”steps” for the purpose of this report. The exploration will consider three steps of different power modulations, that will make up the laser program, throughout the experiment.

1. Firstly, a step with the initial power required to raise the temperature of the surface.
2. Secondly, a step taking place in a small time window, 1 second, with a target power with which the last step should start with.
3. The last step, where a lower power setting is used to maintain the elevated temperature for 10 seconds.

The effect which creates a power modulation similar to the one seen in figure 16. To find the suitable power modulations for the three steps different percentages of the base power of 2000 Watts os used. For each new test made with a disk not previously subjected to testing an emissivity setting of 0.3 is used, if a test is done on a piece that was previously tested a setting of 0.7 is used instead.

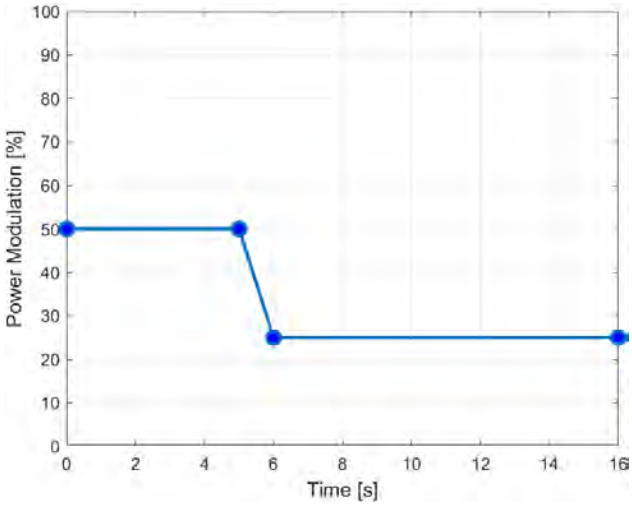

Figure 15: Power modulation in 3 step variations.

UNIVERSITY OF SKÖVDE

3.6 Iteration 3 - Act

Using 14 disks various settings for the three periods are tested. For the first period durations between two and seven seconds with between 75 and 100 percent are used. The seconds period are between 17 and 20 percent settings are tried for one seconds, and for the third period, similar settings as for period two are tested (table 7). Test 55 has a different emissivity setting, 0.7, to test and confirm the variation. Once the 14 disks are spent, some experiments are repeated on used disks with a higher emissivity setting. For this part of the iteration lower powers are explored for 11 experiments.

3.7 Iteration 4 - Plan

In this iteration the effect of heat over time, with possible analysability in photodiode signals, is tested with an two dimensional DoE. The disks used in this iteration are thicker than previous tests, of approximately 10 - 11 mm in thickness, and cut from the same cylinders retaining the same radius and methods for manufacturing. As learned in iteration 1, a preparatory stage can be useful and as such one is implemented in this iteration. With the new thickness of disks, a few effects will change and thusly new tests are required. For example, the thicker material requires more energy to warm up, and they also possibly require more energy to stay at the elevated temperature. Verification of the method for maintained heat from iteration 3 is made, as well as modifications if required. The photodiode sensors are used to gather necessary data for the reflections regarding photodiode signal analysability and correlation to heat dispersion in the material.

As mentioned, the main stage consist of experiments of a more structured manner than the exploratory experiments of iterations 1 through 3. The suggested DoE consist of 12 experiments with four variations of temperature and two of time spend holding the temperature. Because of difficulties related to reaching exact temperatures with this method, a target temperature will consist of a 50 degree range as seen in table 1.

Temperature $[°C]$ \ Time $[s]$	60	120	10
700-749	1	2	3
750-799	4	5	6
800-849	7	7	9
850-899	10	11	12

Table 1: Temperature vs. Time DoE

Once all heat treatments are completed the pieces from this iteration are prepared for material testing. The cross section of interest is located using the thermal imagers documentation of the process to find peak heat values and including them in the section. The material is then moulded into a plastic mould with a Citopress-30 machine, also by Struers. It is then grinded, polished and etched in preparation for hardness testing and microscopy. Following preparation the material parameters are to be extracted and then compared in relation to heat treatment regiment. From the comparison some final conclusions for the method developed in iterations one through four is made using a heat map. In the heat map holding temperatures and times are compared with estimated development of martensite, hardened material thickness, Vickers hardness values, and photodiode signal intensity values.

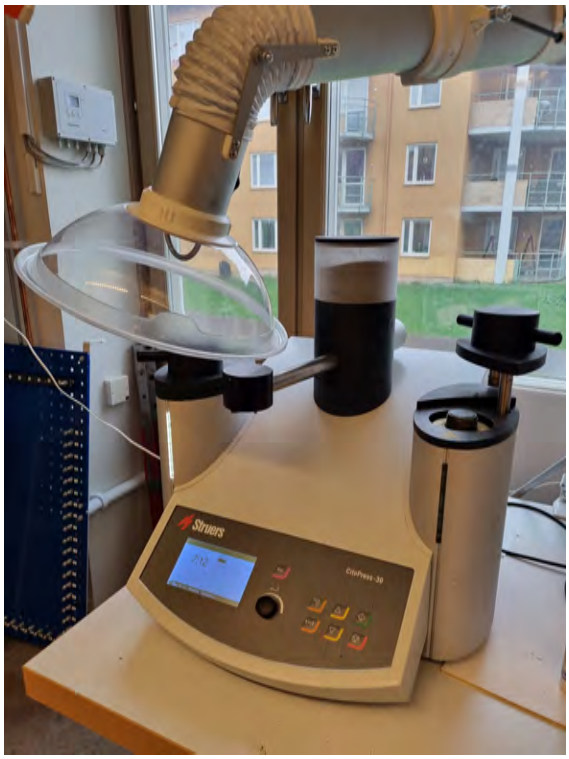

Figure 16: Power modulation with 3 variations.

3.8 Iteration 4 - Act

The act part of this iteration is instigated with cutting and grinding of the thicker test samples. Other than the thickness the samples are prepared in a similar way as in previous iterations, with grinding with 220 grit sand paper and cleaning with gasoline and acetone. 35 pieces are prepared in this way for the experiment. As found in previous iterations, thickness greatly affects the speed with which the head accumulates in the pieces. As such, the first couple of pieces are used to adjust the process to the new thickness. This is done by testing higher powers and P0-values, as greater thickness causes slower heat accumulation (Table 8). Powers ranging from 2000 to 5000 Watts are tested and 5000 Watts are chosen to work with as it produces a suitable temperature elevation speed at high P0-values and suitable temperature holding values at lower P0-values. Once suitable parameters to reach the wanted temperature a spike was observed in the temperature. The same spike was not present in the thinner disks experiments. To examine the heat spikes further some experiments are conducted in an attempt to even out the heat spike with a heat modulation instance gradually lowering the temperature towards the target temperature modulation for hold temperatures. This strategy is tested on previously warmed pieces but is scrapped as it does not have the desired effect. Instead, for the last couple of tests, the heat spike is included as an factor

for this experiment. To achieve the desired effect of rising the temperature and then holding it at an elevated temperature, now including the temperature spike, P0 for the first step is set to 85% for ten seconds. For the second step times exceeding the step maximum time limit of 60 seconds is desired. To achieve this some variance between the steps seems to be required, or the machine activates a full power output of 100% for the remainder of the time the laser is active. To remedy this a minimal variance in the P0-value for the holding steps is included, ranging from 11.9% to 12%. Temperature holding times of 60, 120, 180, and 300 are tested and seven pieces of possible interest are produced.

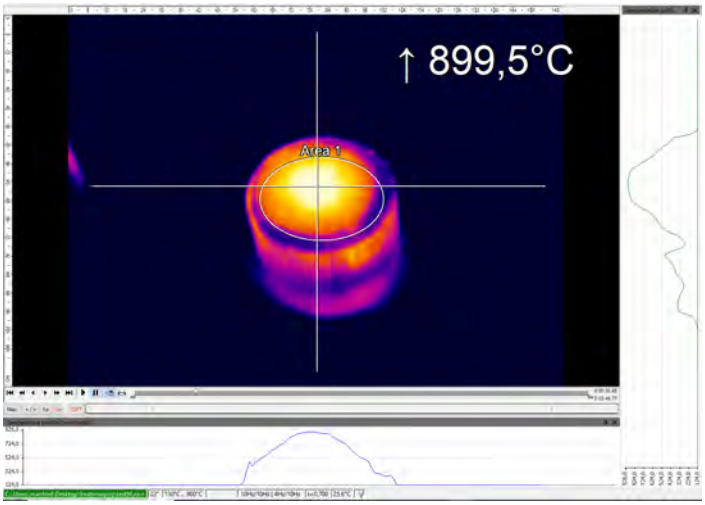

Figure 17: Thermal image showing max temp and temp profiles horizontally and vertically aligned with max temp.

Figure 18: Test sample 96 cut along the documented horizontal temperature profile.

Holding temperatures along the two profiles are documented with the thermal imager (Figure 27). The seven pieces are brought back to the material lab to be prepared for hardness testing and micrography. They are cut to create a cross-section containing multiple testing zones along the horizontal temp profile, minding that the area of interest is the one holding the maximum temperature. Thusly, the cut is placed so that the maximum heat point is at a grinding distance to the cut cross-section (Figure 28). The pieces are then moulded in plastic moulds, grinded, polished, and etched using a 3% Nital solution.

3.9 Iteration 5 - Plan

For this iteration the common theme of the previous iterations is changed. The welded part is moved closer to the focal point and the applied laser has a trajectory across the length of the

piece. The method for laser hardening of CGIs used is modelled after one used by Writzl et al in 2021 [24]. In the paper the researchers use a laser machine with a similar wavelength laser (1080-nm) with Gaussian beam spread of 2 kW maximum power. Even with the slight variance in laser wavelength, the method is assumed to be directly applicable. Thusly, this iteration handles applying their method to the currently written pilot study, as well as including previously used methods for gathering data, i.e. the photodiode sensor and the thermal imager. The method used by Writzl et al includes irradiating the material at three different powers, 400, 449, and 514 Watts, at a defocusing distance of 50 mm and with a travel speed of 5 mm/s. The laser travels across the material in parallel straight lines 2 mm apart and is irradiated with 10 second wait time between irradiations as to not overheat the material. Their paper includes three more differences, one being if the material was nitrided or not. Seeing as nitridation is an expensive and time-consuming process, the option is be omitted in this reproduction of their test, since the overall goal is to cut costs in hardening of CGIs. Another difference is that Writzl et al reports that irradiating at the power of 400 Watts does not cause any martensite to form within the material, as such, powers of 449, 514 and an arbitrarily chosen power 580, are tested. The third major difference is the fact that the CGI used in this project is ferritic while theirs is pearlitic, and thusly possess a greater capability to form martensitic microstructures while hardening.

The three power settings are combined with three levels of travel speeds, 4 mm/s, 5 mm/s, and 6 mm/s to a total of 9 experimental settings (table 2).

Power $[W]$ \ Speeds $[mm/s]$	6	5	4
449	1	2	3
514	4	5	6
580	7	8	9

Table 2: power vs. speed settings

Each of the nine settings is tested in two ways, where one is a single line repeated three times for analysing repeatability, and the other is more similar to Writzl's where five irradiations will be used in succession to create a hardened surface. The second method shows how well the lines combine and gives an estimation of the methods functionality for hardening of surface areas. These experiments are also performed on the 30 mm diameter cylinder material, albeit this time, they are not cut into disks before hardening. Instead they will be performed on the rounded surface with a travel path parallel to the centre axis of the cylinder. Each cylinder has space for 12 and are beforehand grinded manually to receive an even surface quality and thickness throughout the whole cylinder.

3.10 Iteration 5 - Act

For this iteration three CGI cylinders are grinded down manually so that the rounded surface is of uniform quality. The pieces are then washed with gasoline and acetone, and in this iteration they are attached to a turning chuck in the laser machine, as seen in figure 19. Two sets of programs for the laser machine are then made, where both irradiate the surface in 15 mm lines along the cylinder, although one shoots three and the other five. The program that produces three lines does so at angles of 20, 45, and 70 degrees from the starting angle, while the other does so at 2 mm distance apart starting at 7.8 mm from the vertical arrow (Figure 20). The programs are set to produce the lines at an interval that includes a 10 second waiting time between irradiations to let heat disperse, as stated in the paper by Writzl et al. Between runs the parameters are changed according to a randomized order to remove effects of conditional or accumulative factors. Also, before running the next set of parameters, the temperature of the cylinder is allowed to fall below 30°C. By doing so, elevated starting temperatures are not present to affect the outcome of the irradiation. The cylinders with the 18 variations of experiments are brought to the material lab where they are cut, moulded, polished, and etched in a similar manner as the samples from iteration 4.

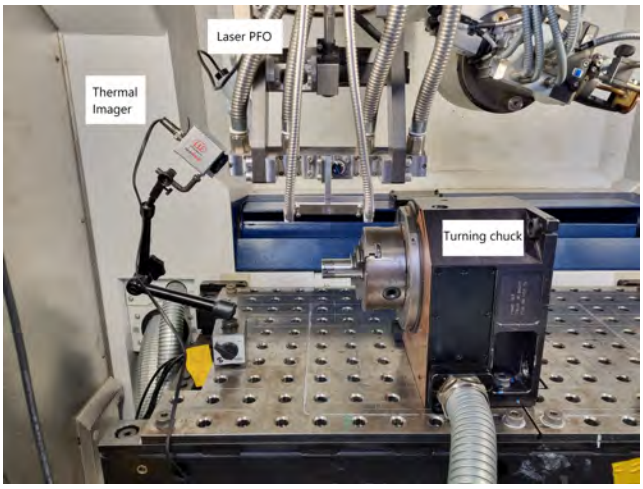

Figure 19: Experimental setup for iteration 5.

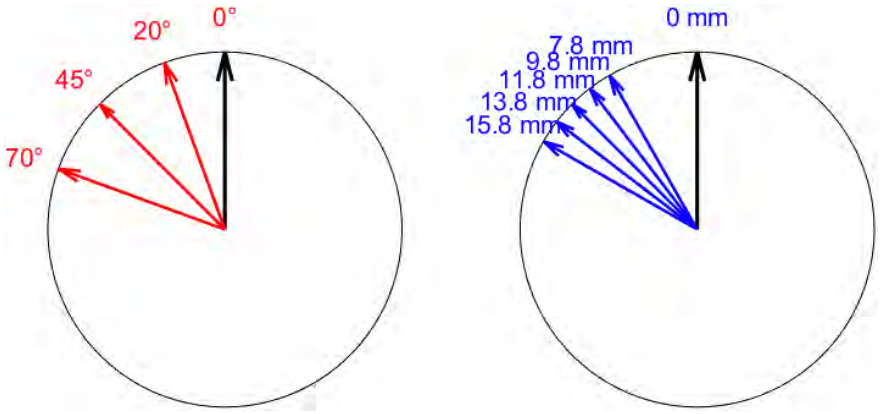

Figure 20: Distances with which the two laser machine programs irradiate with.

3.11 Analysis of Iteration 4 and 5 Data

Similar methods of documentation of data is used in both iteration 4 and iteration 5, even if the retrieved data differ somewhat with the methods. The retrieved data is processed and evaluated with MATLAB, where data of various sorts can be compiled into a larger dataset, as it is in this project. The various data-files from the laser machine process are stored. Images, video, and graphs from the thermal imager, and database-files of the wavelength ranges from the photodiode sensor. As mentioned, the irradiated test samples were brought to the HIS material lab for processing before hardness testing.

3.11.1 Hardness Testing och Microscopy

Hardness testing and microscopy analysis are done with the same machine, a QNESS 60 A+ EVO. Iteration 4 and iteration 5 pieces differ in how they are irradiated, and as such the surface layer differ in location, but for both the cross-sections are made to be able to analyse the depth of the hardened layer (Figure 21).

Figure 21: Assumed location of hardened surface layers in red in cross-sections of iteration 4 (left) and iteration 5 (right).

Areas of interest are tested for hardness to give an understanding of how the irradiation have affected them. If possible mean and max values for hardening are taken, and all images of assumed interest are so as well. The force applied is measured in kgf and a kgf value of 1 is used for all measurements.

3.11.2 Data handling with MATLAB

The database-files from the photodiode sensor are loaded into MATLAB, where the data point arrays from the wavelength ranges are compiled and sorted. They have to be sorted since the

original database-files contain several arrays of 0-value data points, and some that lack importance for this project. Also, the NIR wavelength arrays are originally stored in the reversed chronological order than that of the VIS wavelength arrays. Once the important data is extracted various graphs can be made for feature evaluation of the graphs. Data from the thermal imager are extracted in text dat-files containing temperature and time signature on each line. Extraction of the data is made using a loop and extracting the data line by line into arrays.

3.11.3 Heat Map Construction

For the creation of the heatmap, a method for comparison only used in iteration 5, all ingoing parameters and the resulting values and data is used. Except for the wavelength ranges the parameters and values are mean and max depth and mean and max hardness. Because some of the wavelengths are of relatively small magnitudes compared to others, all values that are compared are normalised so that, for example, each wavelength range or mean depth value is compared individually. The normalised value that is compared is the mean value of the top 1/3 values in each range. While using a minimum magnitude of the interesting arrays from original data fluctuating around 4500. So in equation 1, $max(x)$ is the max value of the highest value of the range, $min(x)$ is the lowest, and all values above 1/3 are included in them mean series.

$$\text{mean} = \frac{1}{N}\sum_{i=1}^{N} x_i \quad \text{where} \quad x_i > (\max(x) - 0.66 \cdot (\max(x) - \min(x))) \tag{1}$$

Once these values are compiled for all wavelength ranges of all test runs, equation 2 is used to normalise the values per parameter results and ranges, making the lowest value 0% and the highest 100%

$$\text{normalised values} = \frac{(y - \min)}{\max - \min} \cdot 100\% \tag{2}$$

The data is then compiled using the "colormap" function included in MATLAB, which creates heat maps with the possibility to choose what colours are included.

4 Results

This section handled the result and reflection of the five iterations (Figure 10). The method section of this paper includes subsections on the five iterations and a sixth on the analysis and handling of the data. However, in this section on results, the results from the data handling will be included in the iteration where the data was created.

4.1 Iteration 1 - Reflection

The first iteration included work done in preparation of the remainder of the project. It included making the fixture, investigating how and if the beam modulation could be used when irradiating a surface when the laser optical source is placed at a greater distance than the focal length, and trails to find a suitable emissivity setting for the thermal imager. The fixture was made in a simple manner, where a 30 mm diameter and 1 mm deep slot was machined from a $20x15x5$ $[mm^3]$ slab of steel. It was assumed that a simple fixture would be sufficient to hold the disks in place, taking into account that the disks expands when heated. Modification of the laser beam modulation between CF and RF does not have any significant consistent and observable effect on the heat signature. In figure 22 two different heat profiles can be seen, both overlapping the same position in two different experiments. Both are irradiated with the same parameters up until the time of the heat signature seen in the figure, which happens just after the initial heat peak has calmed down (Table 8). One of the experiments show a central peak while the other display a dip in heat in the middle.

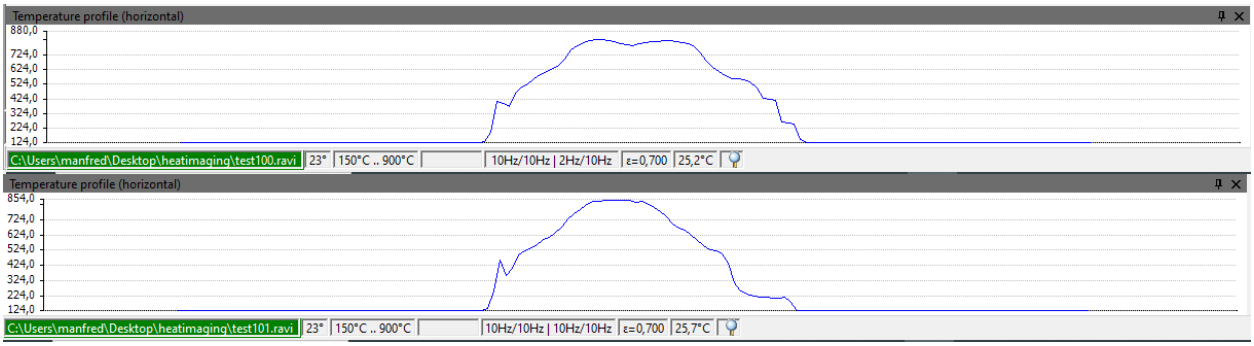

Figure 22: Horizontal temperature profiles of tests 100 (above) and 101 (below).

These tests are documented in iteration 4, but show the same phenomenon as was observed in iteration 1. Because this inconsistency doesn't occur often, the beam modulation is set to 100% irradiation through the RF, to see if it happens more throughout the study. In tests 24 and 29 (Table 5) temperatures with very similar peaks were observed in both the thermocouple data and the thermal imager data, deviating only 5°C for 24 and 43°C for 29. Test 24 was recorded with an emissivity setting of 0.3 on a disk not having been previously irradiated, while an emissivity setting

of 0.7 was used for test 29 which had been previously irradiated. Worth noticing is that test 24 was heated to around 250°C and 29 to around 525°C, and thusly the test omits information on emissivity on temperatures between 700 and 900.

4.2 Iteration 2 - Reflection

In the second iteration the temperature and distance between irradiated surface and laser optics is examined to find a heat signature of the beam that is suitable for the project in relation to the shape and size of the top side of the disk. Three different heights was tested, but after testing the initial added height of 310 mm was deemed as the most suitable of the three since it covered almost the whole top surface while not directly irradiating the fixture. Additionally, the height in combination with a power of 2000 Watts made the values achieved with the P0-value setting manageable within the wanted range. However, using the disks of varying thicknesses, surface temperature as a result of irradiation at 2000 Watts for any specific duration also show substantial variation. Raising the power from 0 to the P0-value in a four different times was tried, creating even more variations depending on the set power and P0-value (Table 6).

With some suitable initial power modulation steps to choose from, the remaining tests performed in the iteration were aimed at finding settings that would make holding temperatures possible. The fourth test was able to hold a temperature with low variation, between 609°C and 623°C, for 5 seconds. This ability to hold the temperature, however brief, was seen as evidence that the method could work, and thusly it promoted further testing in the next iteration (Figure 23).

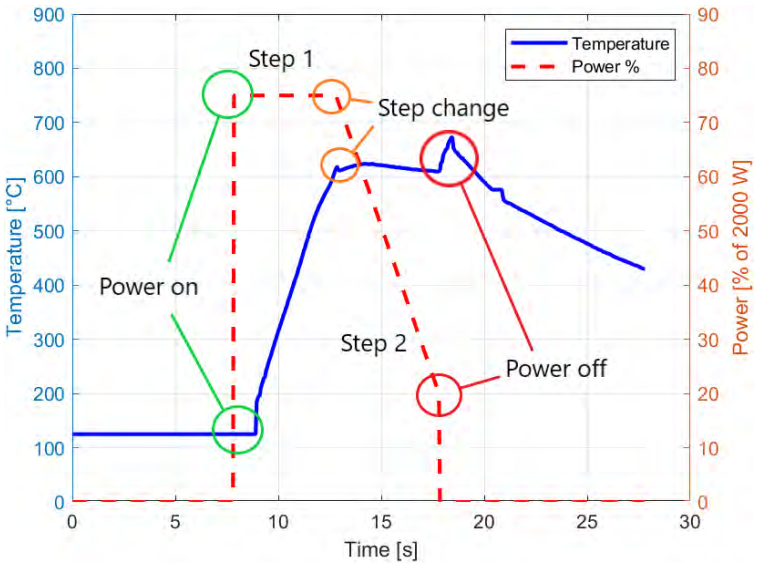

Figure 23: Power modulation vs. temperature of test 45.

4.3 Iteration 3 - Reflection

In the third iteration focus lay only on attempting to understanding and finalizing the method with which to hold the temperatures for extended periods of time. Whilst working through the batch of test disks it became clear that the temperature gain and retention was heavily dependant on the thickness, and more so the shape of the part being irradiated, due to differing heat dispersement properties of different shapes. Thinner disk became hot faster and vice versa. The introduction of a middle step for lowering the P0-value in a relatively short time was introduced, making holding percentages easier to pinpoint. Moving through various combinations resulted in a final successfully held temperature between 316°C and 341°C for 10 seconds (Figure 24). However, test 58c was a previously irradiated disk and the temperatures reached where relatively low compared to the 700°C to 900°C interesting interval. To achieve higher temperatures longer periods of irradiation is assumed to be the better choice compared to higher powers for later iterations.

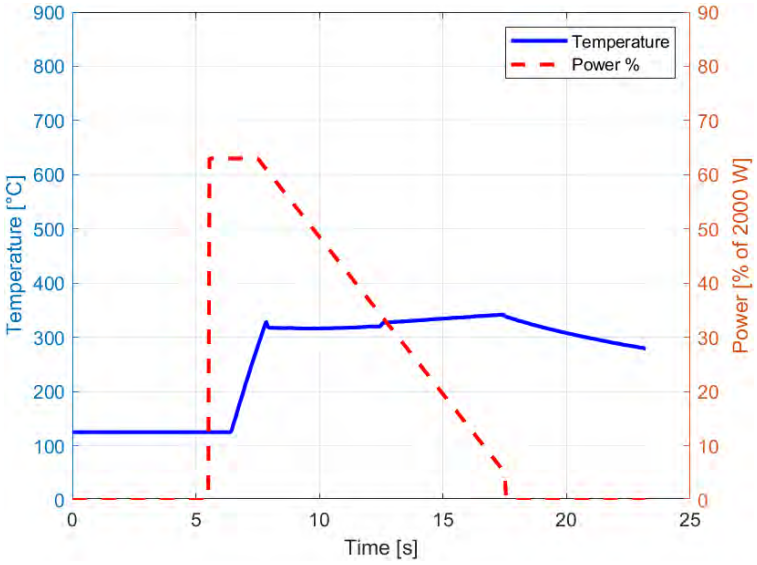

Figure 24: Power modulation and temperature of test 58c.

4.4 Iteration 4 - Reflection

The thicker test samples used in iteration 4 required a higher power to reach the target temperature in similar time frames as the ones previously used. As stated in the act section for iteration 4, 5000 Watts was well suited for the task. After the power was established, new tests to find what P0-values elevated the temperature to between 700°C and 900°C was performed. The test samples where of similar thicknesses, varying between 10 mm and 12 mm. Compared to the thinner disks, the thicker

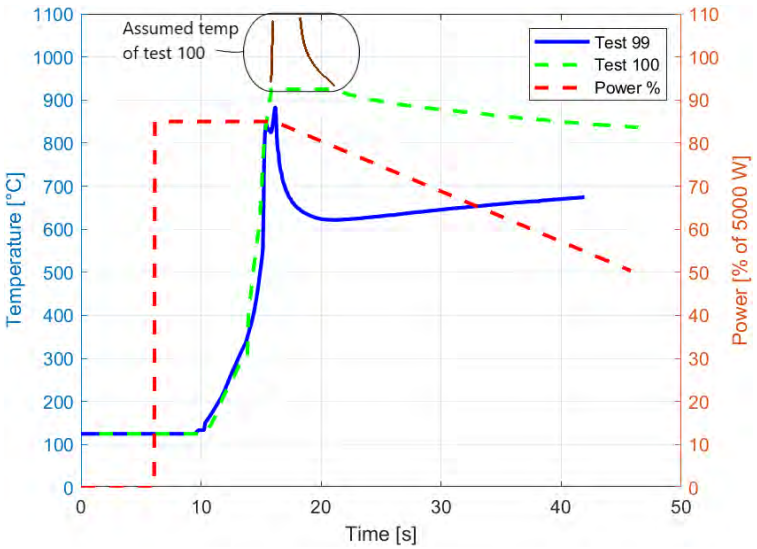

Figure 25: Comparison between test 99 and test 100.

test samples are less exposed to the effects of small variations of thickness. However, as it seems, not so much as to prevent large variations in surface heat retention. For example, both tests seen in figure 25 are made using the same power settings, power modulation, surface treatments, but with a small variation in thickness (Table 8). Assumably, the problem would not be as prevalent when treating larger work pieces, as variations in heat retention properties would affect the process less, while still requiring more energy to achieve the same temperatures.

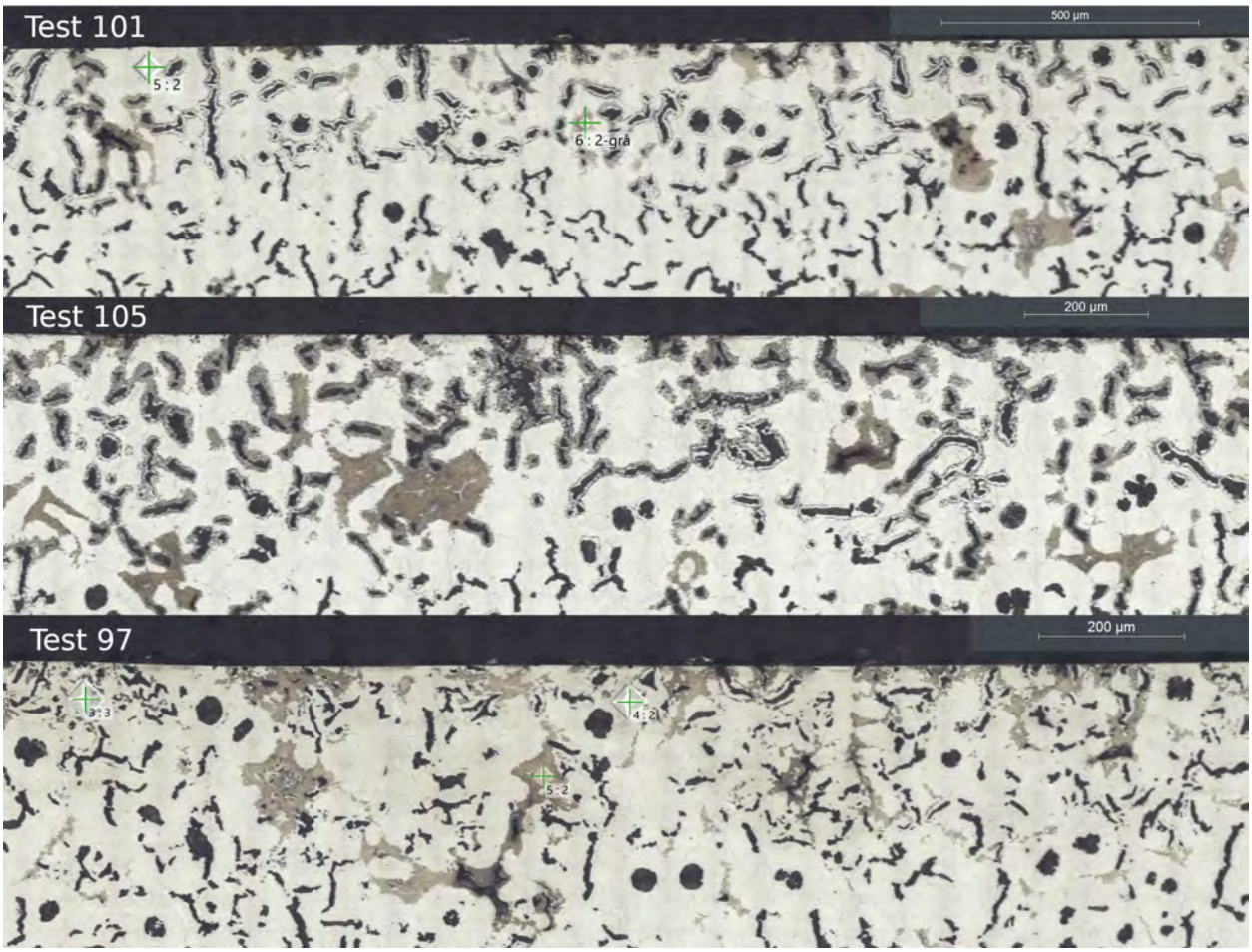

Figure 26: Microstructure near surface of tests 101 (above), 105 (middle), 97 (below).

As is, in iteration 1 through 4 a method similar to a more traditional heat treatment is explored. From the large amount of test samples six was analysed through microstructural analysis and testing of Vickers hardness. No complete temperature dependant transformation of the matrix was achieved in the 60 (test 101), 120 (test 105), or 180 (test 97) second holding times that was used (Figure 25)(Table 8). However, as can be seen in figure 25, what seems like time dependant growth of darker grey areas take place. Most probably this is due to carbon migrating from the graphite

deposits into the iron matrix, austenitisation, as was discussed in the theoretical background section of this report. These areas are of greater hardness than the brighter uneffected areas that, in hardness and appearance, seem unaffected by the elevated temperatures.

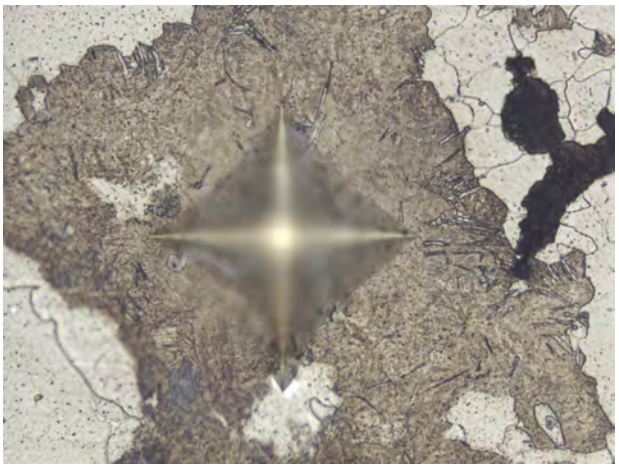

Figure 27: Vickers indent in darker area of test 97.

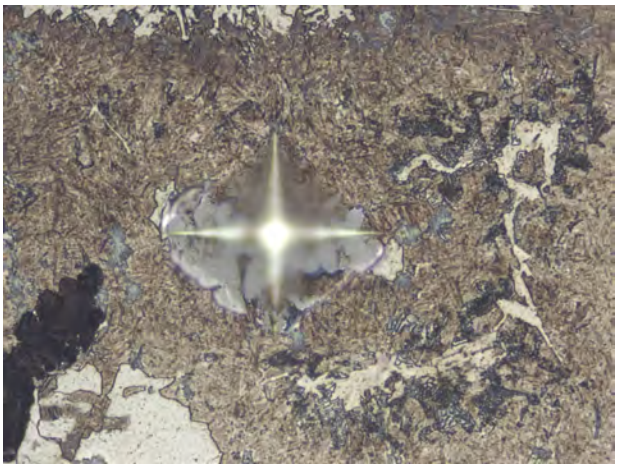

Figure 28: Vickers indent in darker area of test 101.

While the substrate material has a hardness measuring to around 150 HV, the hardness of one grey area of test 97 and one of test 101 were measured to be 445 HV and 739 HV, respectively. So, even if heat build up in the test samples led to low cooling rates, hardness were still elevated in these areas. Tests 101 and 105 held a slightly higher temperature than test 97 for the duration of the test, with means of 875°C and 825°C, which could be the cause of the differences in how quickly the areas propagated in the iron matrix. If the holding times would be extended over a longer than 180 seconds, based on these experiments and on a paper by [16], the ferrite matrix of the interesting volume should transform into ausferrite. Further analysis would be needed to find out if the grey material has a martensitic structure or not, albeit the low cooling rates of the test samples shows a reversed correlation with the hardness values. Ausferrite in test 97, which held the temperature of around 875 for 180 seconds and cooled down with a mean rate of $-21.2°C/s$ showed the hardness value of 445 HV. While ausferrite in test 101, holding a temperature of 825 for 60 seconds and a mean cool down rate of $-14.7°C/s$, showed the higher hardness of 739 HV.

Considering the similarity of the test runs, where the same laser settings where used for the three runs (97, 101, and 105) (Table 8), the first 60 seconds of the runs should also be similar. To make any kind of final conclusions from the data, seen in figure 41 and figure 41 on the process would be premature in this stage, however, some process seem to start at the 40 second mark which causes drastic changes the light emission output of the process. The images seen in figure 29 show 4 heat signatures in the process corresponding to the 30 s, 40 s, 50 s, and 60 s mark of

the photodiode data. Marginal migration of heat from the centre and outwards can be observed, however large fluctuations like these should not stem from temperature alone, especially since the target temperatures are achieved well before before the 30 s mark.

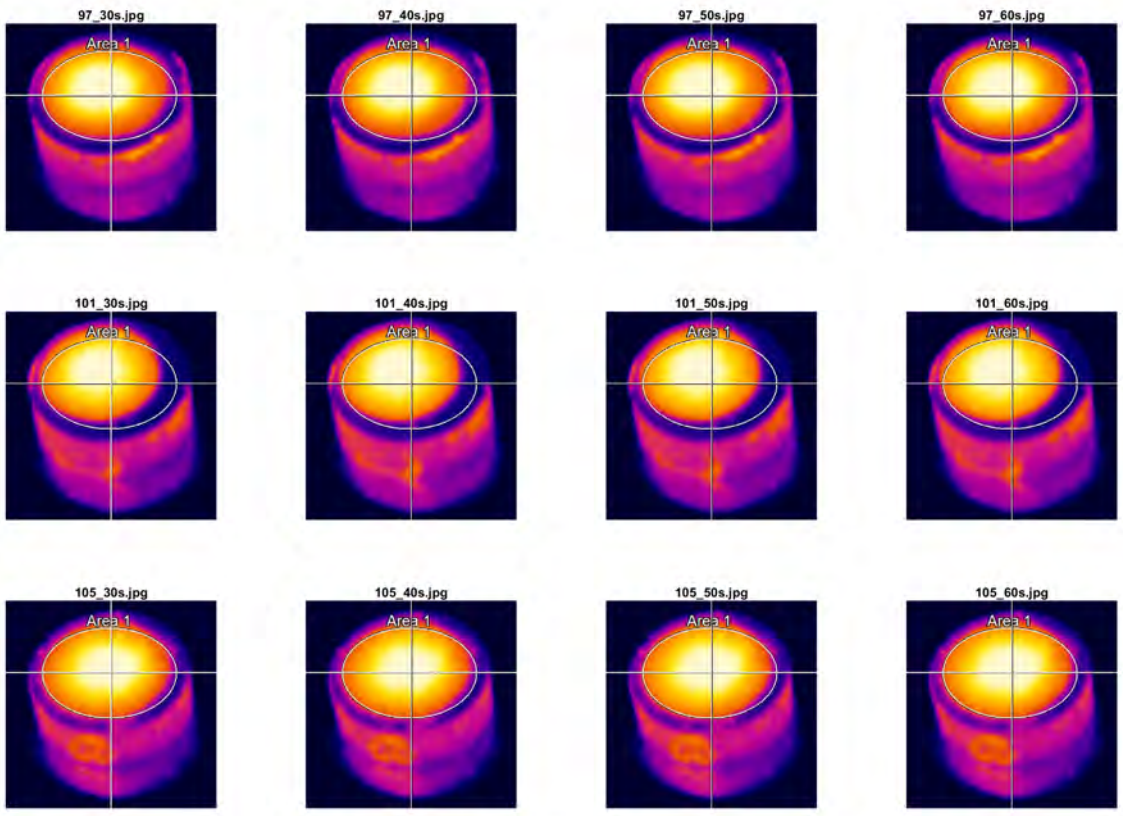

Figure 29: Images of heat signatures after 30 s, 40 s, 50 s, and 60 s of irradiation.

From figure 41 figure 30 and 31 is derived, which shows how much the various wavelength starting condition as a mean value, as well as how and how much they change. A possible correlation can be made to the growth of ausferrite in the matrix. The higher starting signals in the visible spectrum of the photodiode data (Figure 30) could be derived from the purity of the untreated ferritic matrix, as pure iron mainly emits radiation in the very same air wavelength range, 218 nm - 646 nm [34]. Possibly, the change in the photodiode signal can stem from the change from ferritic to ausferritic matrix, as suggested by Palmer, Elmer, and Babu [33], although further investigation into the matter would be needed to establish the correlation with the gear used at HIS. No strong prominent events are observable as the temperature rises in the first 10 seconds. Test samples 101 and 105 has a higher light emission output than test 97 (Figure 41), which does not correlate to the thickness of the pieces, but possibly to the irradiated surface's finish before irradiation.

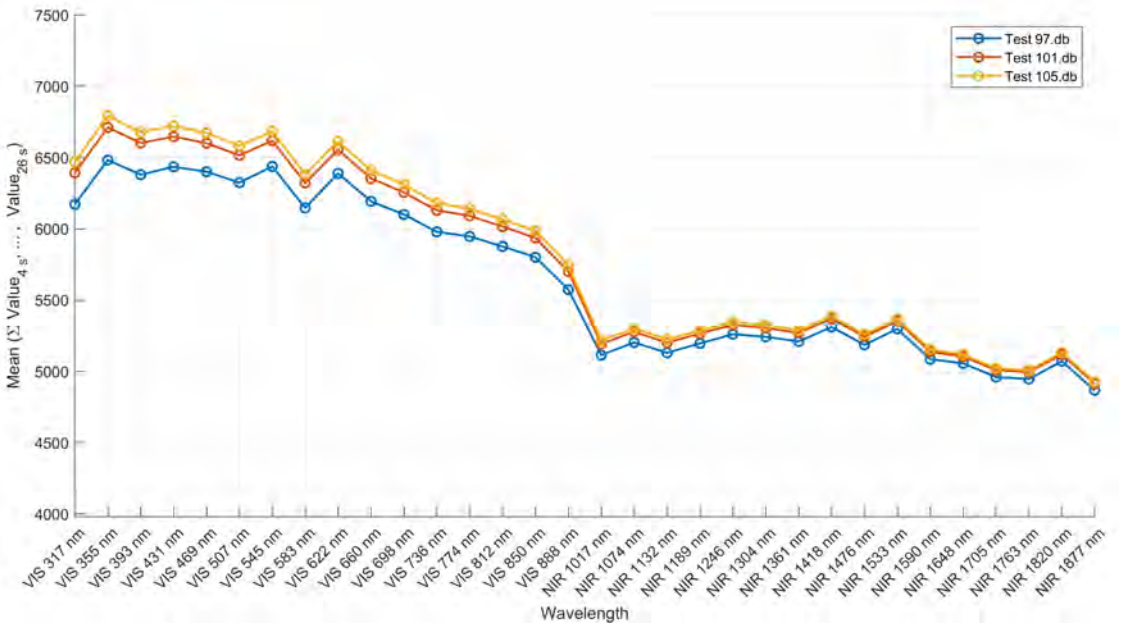

Figure 30: Wavelength mean value for data points between 4 second mark and 26 second mark for tests 97, 101, and 105.

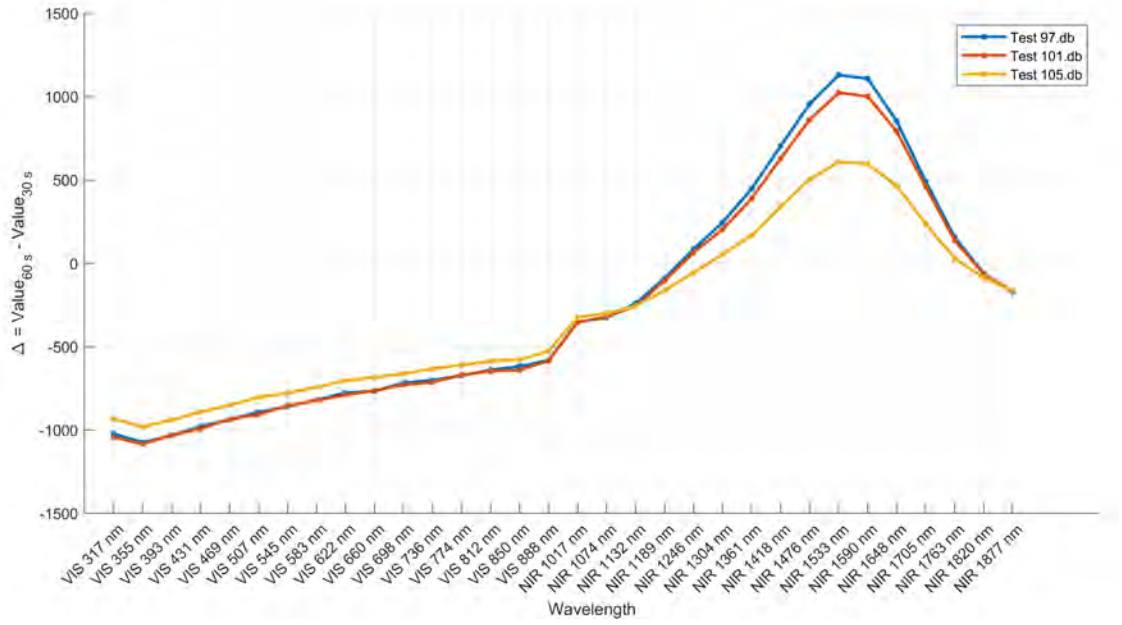

Figure 31: Change in smoothed light emission value by wavelength between 30 s and 60 s for tests 97, 101, and 105.

UNIVERSITY OF SKÖVDE

4.5 Iteration 5 - Reflection

The fifth iteration of the project was performed according to the plan with less exploratory manner than the previous iterations. This was because the Writzl et al. [24] paper had provided a starting point and part of the iteration handled confirming the laser machine settings related to that starting point. What's more, all gear for preperation and gathering data had already been used, and thusly, was easily applicable to the new task. No mayor difficulties occurred other than in the initial settings for the photodiode sensor, meaning that some of the tests was remade to avoid overly unmanageable data. The measured temperatures with the method of irradiation used in this step more often than not were raised above the 925°C (Figure 43). This again means that the peak temperature is above the range measurable with the thermal imager. However, some the samples in the range that received the greater amount of energy per area achieved above melting temperatures, like samples 9a and 9b seen in figures 32 and 33, respectively.

Even if the thermal imager data does not provide any useful information of temperature peaks, other than than showing that 449 Watts of laser machine power may be to low to cause meaningful change in the material, it does show the steep cool down rates. In some most cases temperature cool down rates area measured to be around $-1000°C/s$, which should raise awareness of the risk of cracks nucleation. The test samples from iteration 5 was also cut, grinded, polished and tested for Vicker's hardness in the same way as the samples from iteration 4 (Figure 34).

Figure 32: Test sample 9a.

Figure 33: Test sample 9b.

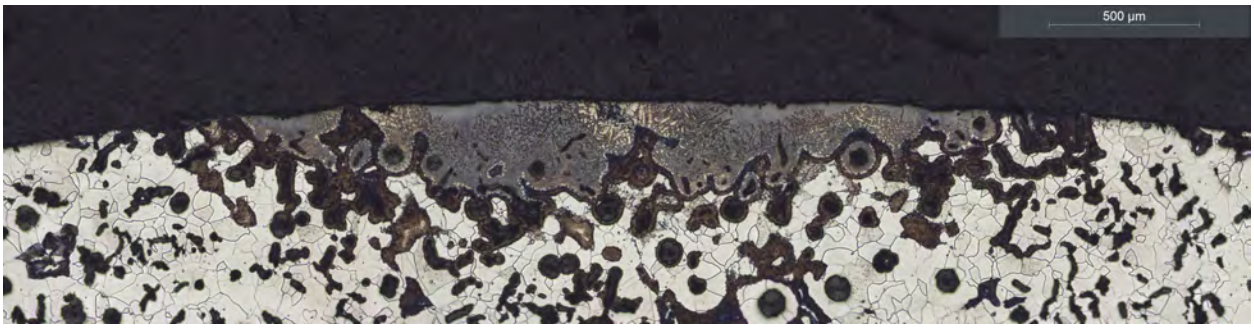

Figure 34: Cross section from test 9a.

Test	Power	Speed	Depth Max	Depth Mean	HV Max	HV Mean
1a	449	6	0	0	150	150
2a	449	5	0	0	150	150
3a	449	4	0	0	150	150
4a	514	6	0	0	306	233
5a	514	5	0.11	0.07	463	267
6a	514	4	0.10	0.10	799	730
7a	580	6	0.21	0.17	721	578
8a	580	5	0.26	0.23	951	815
9a	580	4	0.38	0.33	962	851
1b	449	6	0	0	150	150
2b	449	5	0	0	150	150
3b	449	4	0.11	0.04	520	200
4b	514	6	0.15	0.08	752	483
5b	514	5	0.27	0.23	887	731
6b	514	4	0.34	0.27	915	836
7b	580	6	0.25	0.19	934	795
8b	580	5	0.29	0.21	938	787
9b	580	4	0.54	0.38	917	849

Table 3: Test results including power, speed, melt pool thickness, and hardness.

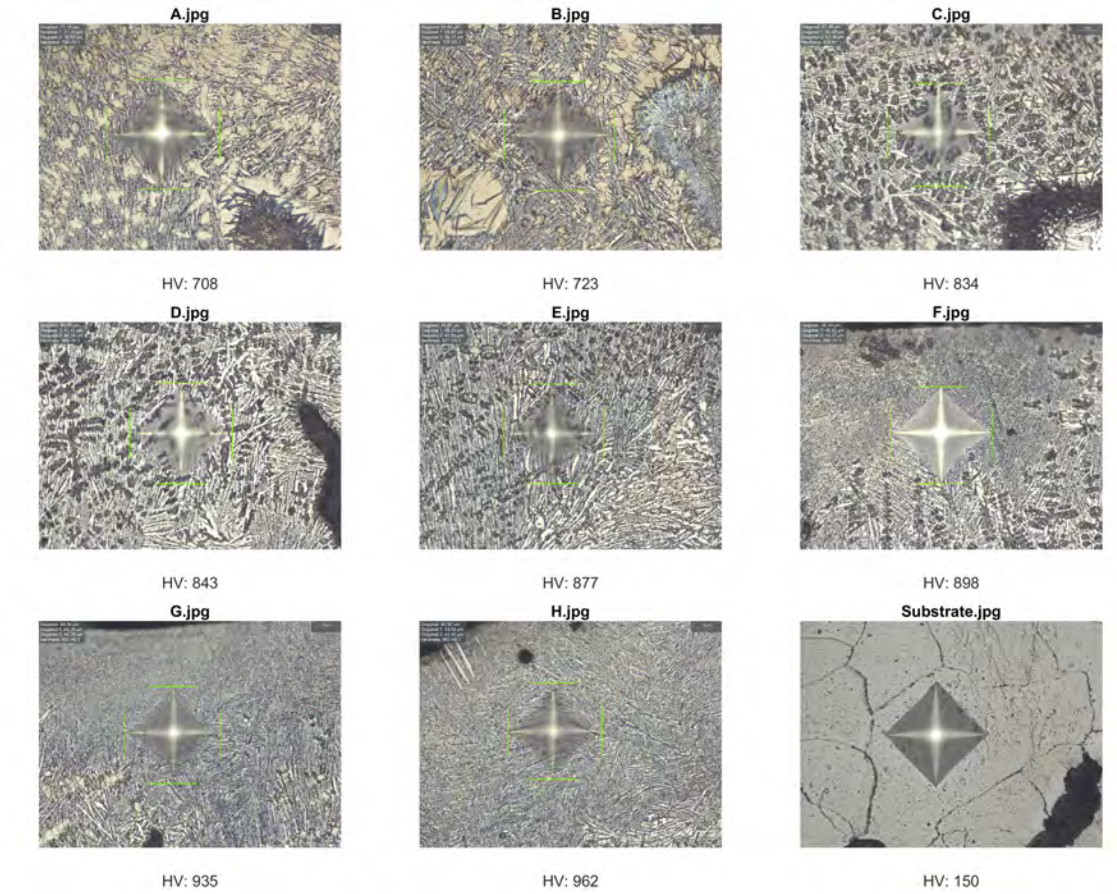

Figure 35: Images from hardness measurements in iteration 5.

The results of the hardness testing can be seen in table 3) where it is also obvious that the samples irradiated with a slower traversing beam of higher power creates surfaces of higher hardness and with greater depth, keeping the unanimously fast cool down rate in mind. Hardness values in the tests were heavily linked to how the structure looked at the micro-scale. As seen in figure 35 depicting some of the hardness measurements locations and surrounding area, three different microstructures are noticeable, not counting the substrate seen in the ninth image. Images A and B shows bright cores separated by laminar laths of martensite [35], and HVs of 708 and 723. C, D, and E show darker cores and with more martensite, with HVs of 834, 843, and 877. C with the HV 834 shows some traces of the brighter cores with lower HV, suggesting the matrix is in some stage of transformation between the two phases granting it a middle value in hardness. F, G, and H which are located closer to the irradiated surface show a uniform structure of martensite and HVs of 898, 935, and 962. With the lower valued images F and G being measured in areas close to darker or brighter nodules than image H. A being measured furthest from the surface closest to the location recieving the highest irradiation, and H closest. The same connection between structure and hardness values was seen throughout all of the measurements. Similar structural results was achieved with similar irradiation method, albeit with another cast iron verity, by Al-Sayed et al. [36]. These result do however differ from the Writzl paper [24], where martensite was seen when irradiating with 449 Watts at a speed of 5 mm/s. The pearlitic material used is, as mentioned, more prone to develop martensite, possibly contributing to the varying results.

The retrieved photodiode data shows some notable differences from the data retrieved from iteration 4. Other than the obvious different time frames of the irradiations the fact that the whole runs are comparable and therefore useful also change the approach made to the analysis. Like in iteration 4 the data was divided into wavelengths and compare between the different tests (Figure 48), where observable similarities repeat between the wavelengths. as laser is turned on for a longer time, a sinusodality becomes prominent, with 3 peaks for the 4 mm/s tests, 2 peaks for the 5 mm/s tests, and a single peak for the 6 mm/s tests. From figure 48 and figures 37 and 38 it seem that the signal around 1017 nm is less prominent. This is because the laser is operating around the same frequency so it is filtered not give of values from the laser light source. However, in figure 36 it is possible to observe the same shapes, albeit with a lower wavelength magnitude. The same behaviour observed around the laser wavelength of 1030 nm has been observed in previous experiments made with the same photodiode sensor and laser machine setup. Similar experiments have been made by the HIS research team where the data from the photodiode sensor was used as training

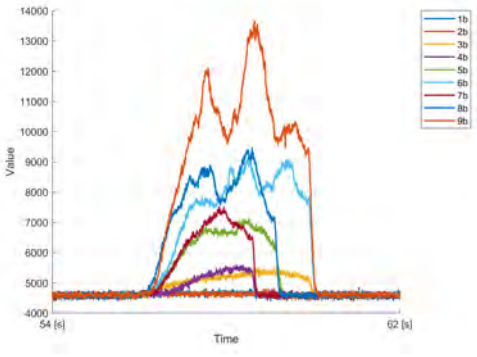

Figure 36: Wavelength 1017 nm of tests 1b - 9b.

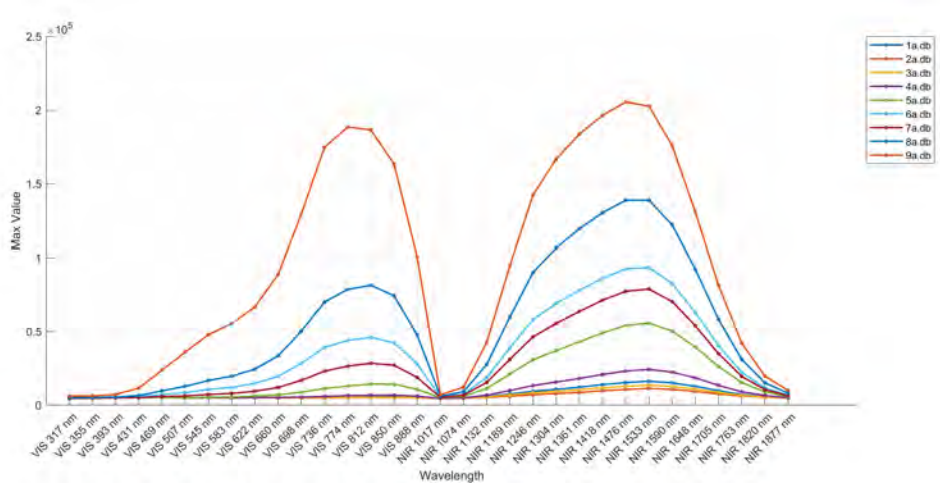

Figure 37: Peak values in 32 wavelengths for tests with 3 lines.

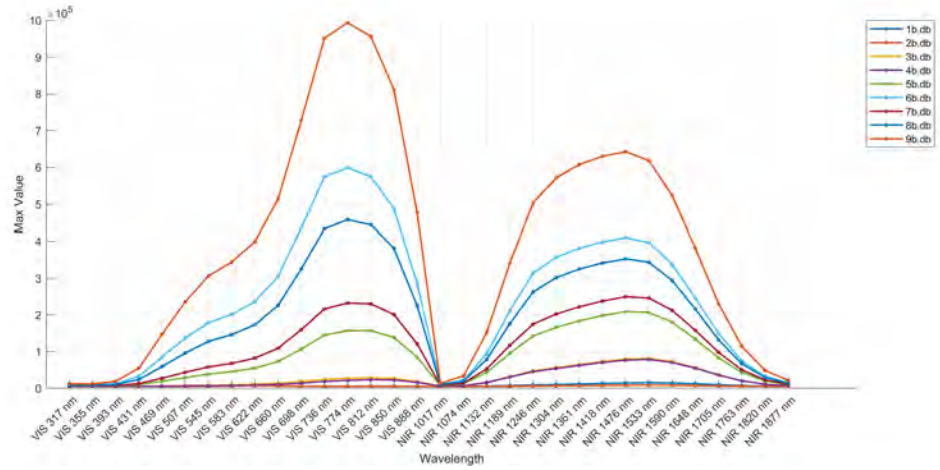

Figure 38: Peak values in 32 wavelengths for tests with 5 lines.

and validation data for a machine learning network for predicting laser welding process events. Often in such cases process events are tied to time codes rendering the magnitudes of the individual wavelength values less important, but rather if some event can be interpreted by photodiode values. As the wavelength graphs show similar patterns which are assumed to correlate more with power and perhaps some natural fluxion of the irradiation case of iteration 5, unlike the signals observed in iteration 4, the magnitude was assumed to hold greater interest.

As observed in figures 37 and 38, and mentioned in regard to figure 36, the signals intensities are of varying magnitudes but of similar graph shapes. In figure 39 all columns are normalised as to

inform on the variations of the wavelength regardless of magnitude. Based on the variations seen in the heatmap, the wavelength of 1017 nm displays a similar relative magnitude as those of the other NIR wavelengths. Furthermore, from the heatmap, we can see that a higher mean in the top 33% are more dependant on the travel speed than it is of the laser power output. This is distinguishable since the wavelength magnitudes of test sample 6b is higher than the wavelength magnitudes of 8b, which is of higher power and fast travel speed. As the hardness measurements and relative depth are heavily dependent on location of the measurement points, they must be assumed to be less precise, even so, measurement of hardness, both max and mean, of 6a - 9a and 5b - 9b are all close to the maximum value. 7a, which is of max power and travel speed has lower hardness in the bunch. Overall, the light emissions of the samples with 3 lines have produced a lower mean magnitude of light emissions than the samples with 5 lines. This may stem from the fact that the process includes irradiating already irradiated surfaces, judging by the trend of larger growing magnitudes for each consecutive line of the samples with 5 lines compared to the samples with 3 lines (Figure 47 and 48).

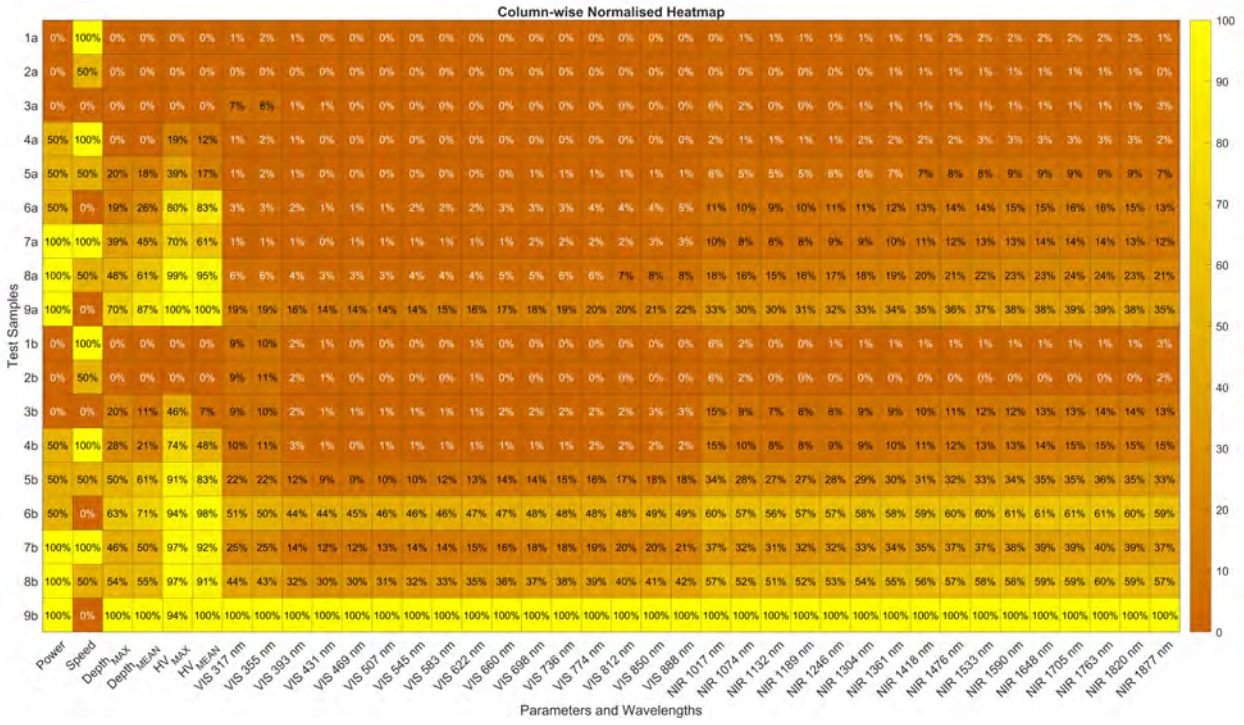

Figure 39: Heatmap for comparing normalised values of parameters and wavelengths.

When performing the hardness tests, some of the samples cracked from the procedure, especially when testing in the hardest and more uniform of the microstructures mentioned earlier (F, G, and H och figure 35). Brittleness of the matrix is also shown close to the graphite nodules, which act as crack nucleation sources [27].

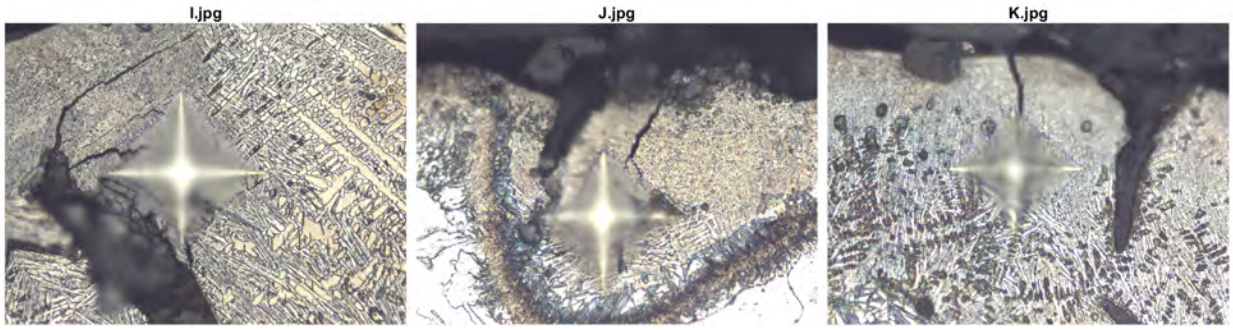

Figure 40: Three images showing crack nucleation in the hardened matrix.

5 Discussion

the decision to use the Action Research approach to this project was made to get a hands on practical start, which it also did. Having the stages - plan, act, reflect - as a template gave the wanted freedom to start working with the experiments in an exploratory way while working with the literature review of the project in parallel. It also provided a clear view of what areas held interest for said literature review. The combination of Action Research and Rapid Literature Review approaches did not cause any major difficulties but rather had complementary functionality. Arguably, having conducted a more through literature review may have changed the approach to the project, like it did when the paper containing the method used in iteration 5 was discovered. However, in does so some other area could become lacking, as is with short projects like a master thesis. And as this project has been a pilot project, I feel the approach have had a good effect towards exploring the base features of the larger project it has been involved in. Working through the iterations it became obvious that the method used in iterations 1 through 4 was hard to get to work in any useful way under the circumstances. Perhaps using a "top-hat" welding modulation would have made it more useful, but seeing as this option was not available this is only speculation. What's more, while the surface was irradiated irregularly, the time spent under irradiation was not long enough to get a good grasp on the how the ausferrite would propagate through the material. One of the more prominent problems with the method was the fact that I would have to program the laser program ahead of time with no possibility for controlling the processes in situ. If the heat development becomes to large, the experiment fails as the parameters fail. Even now iteration 4 required very large tolerances to allow for the fluctuation of temperature. Larger pieces would possibly allow for more heat dispersion and by that also allow for longer periods of irradiation. It would also be fair to assume that larger work pieces would lower variation in other factors, like in the shape of the work piece. Where now, all of the experiments that were used in the final analysis used the same parameters but varied a lot, and a clear majority of the experiments made with the same parameters were not useful.

For iteration 5 however, the irradiation process was less sensitive. The method used could easily be modified and implemented. This was because, as opposed to the method used in iteration 4, the process parameters of power and travel speed were the only factors, while the method in iteration 4 introduced multiple factors. One of which was the success of the power modulations affect on the temperature. It is possible that the same factors were present in iteration 5, but without the same requirements for a successful experiment. The original method from the Writzl paper had martensite development at lower irradiation rates, but instead with pearlitic CGI.

UNIVERSITY OF SKÖVDE

6 Conclusions

The conclusions section of the paper is divided between conclusions of iteration 4 and 5.

6.1 iteration 4

A small amount of ausferrite development could be observed from the material analysis of the iteration 4 test samples. The development seemed to be time and temperature dependant as one would presume, but the process was halted before large volumes could be transformed. Transformation started to happen before the 60 second mark at 850°C and transformed areas reached hardness of between 400 HV and 700 HV. Cool down rates were measured to around $-15°C/s$. At around 30 seconds into the process the photodiode VIS signals started to degrade in magnitude while the ones in the NIR spectrum generally grew. This behaviour was seen in all analysed test samples.
This method uses the laser continuously for several minutes, so without further testing the energy savings made with this method are questionable. Furthermore the lasers ability to develop surface heat is highly inaccurate as the same laser settings can produce widely different results.

6.2 iteration 5

The complete melted areas were produced held the highest HV values. Various hardness could be tied to microstructural characteristic features in the range between 700 HV and 1000 HV. Cool down rates were measured to around$-1000°C/s$. All of these microstructural characteristics contain martensite and higher concentrations show higher HV values. Higher hardness areas also have a tendency for crack nucleation.
The heatmap shows that travel speed have a large influence on wavelength range magnitudes, as well. It also reveals that all wavelength ranges contain useful information even if they seem relatively small compared to others. Furthermore, depth and hardness values scales with energy retrieved while the lowest powers hardly affect the CGI at all.

UNIVERSITY OF SKÖVDE

7 Future work

This study handles somewhat new synergies between CGI, laser heat treatment, and photodiode sensor usage. As such it holds potential to stretch further than the three year period allocated for the larger project it is included in.

The larger project will explore this synergy, with heavier focus on using the photodiode sensor as input data for simulation and various AI-tools. In this attempt, the knowledge that all wavelength ranges holds data of various magnitudes should be remembered. Furthermore, as this study have been able to provide indications of possible control of hardness by achieving various microstructures, more parameters of the microstructures should be explored. Maybe the softer ones of around 750 HV holds a greater resistance to crack nucleation and/or greater sliding wear resistance. If so, further heat treatments for annealing the material may be unnecessary. That saying, I would suggest using the method from iteration 5 in the larger project, however it should be done so on larger work pieces where the heating can achieve a steady state in the relationship between energy received and dispersed.

In a case where iteration 4 is developed further, a "top-hat" welding optics spread should be attempted instead of the Gaussian spread used in this study. This would require a costly change of hardware. After this a more controlled process should be possible, perhaps even when using Writzl's method. If the attempts made with the Writzl's method to achieve a single irradiation to create a hardened surface of high wear and crack nucleation resistance fail, the method from iteration 4 may be attempted to anneal the hardened material toward the same end result.

UNIVERSITY OF SKÖVDE

References

[1] B. J. Oates, M. Griffiths, and R. McLean, *Researching information systems and computing*, second edition ed. SAGE.

[2] K. Säfsten, *Forskningsmetodik: för ingenjörer och andra problemlösare*, upplaga 1 ed. Studentlitteratur.

[3] G. I. Susman and R. D. Evered, "An assessment of the scientific merits of action research," no. 2, pp. 135–161. [Online]. Available: https://www.medra.org/servlet/MRService?lang=ita&hdl=10.3280/SO2022-002006

[4] B. Smela, M. Toumi, K. Świerk, C. Francois, M. Biernikiewicz, E. Clay, and L. Boyer, "Rapid literature review: definition and methodology," vol. 11, no. 1, p. 2241234. [Online]. Available: https://www.ncbi.nlm.nih.gov/pmc/articles/PMC10392303/

[5] S. Kang and J. Shin, "The effect of laser beam intensity distribution on weld characteristics in laser welded aluminum alloy (AA5052)," vol. 142, p. 107239. [Online]. Available: https://www.sciencedirect.com/science/article/pii/S0030399221003273

[6] C. Nordling, *Physics handbook: for science and engineering*, ninth edition ed. Studentlitteratur.

[7] N. Shanmugam, G. Buvanashekaran, and K. Sankaranarayanasamy, "EXPERIMENTAL INVESTIGATION AND FINITE ELEMENT SIMULATION OF LASER BEAM WELDING OF AISI 304 STAINLESS STEEL SHEET," vol. 34, no. 5, pp. 25–36. [Online]. Available: http://doi.wiley.com/10.1111/j.1747-1567.2009.00552.x

[8] W. r. Leijon, *Karlebo Materiallära*, 15th ed. Liber.

[9] J. Volpp, "Laser light absorption of high-temperature metal surfaces," *Heliyon*, vol. 9, no. 10, p. e21021, Oct. 2023. [Online]. Available: https://linkinghub.elsevier.com/retrieve/pii/S2405844023082294

[10] C. Wang, W. Suder, J. Ding, and S. Williams, "Parametric study of melt pool geometry in hybrid plasma arc-laser melting process for additive manufacturing application," *Welding in the World*, vol. 67, no. 4, pp. 923–934, Apr. 2023. [Online]. Available: https://link.springer.com/10.1007/s40194-023-01476-9

[11] G. Lupo, M. Niemann, C. Goniva, W. Szmyt, X. Jia, and V. Turlo, "Modeling of laser beam absorption on rough surfaces, powder beds and sparse powder layers," *Results in Physics*, vol. 67, p. 108043, Dec. 2024. [Online]. Available: https://linkinghub.elsevier.com/retrieve/pii/S2211379724007289

[12] H. Mustafa, M. Mezera, D. Matthews, and G. Römer, "Effect of surface roughness on the ultrashort pulsed laser ablation fluence threshold of zinc and steel," *Applied Surface Science*, vol. 488, pp. 10–21, Sep. 2019. [Online]. Available: https://linkinghub.elsevier.com/retrieve/pii/S016943321931373X

[13] File:iron carbon phase diagram.svg - wikipedia. [Online]. Available: https://commons.wikimedia.org/wiki/File:Iron_carbon_phase_diagram.svg

[14] Steel | composition, properties, types, grades, & facts | britannica. [Online]. Available: https://www.britannica.com/technology/steel

[15] A. Krzyńska and A. Kochański, "Austenitization of FerriticDuctile Iron," *Archives of Foundry Engineering; 2014; No 4*, 2014. [Online]. Available: https://journals.pan.pl/dlibra/publication/102292/edition/88326

[16] R. Ghasemi, I. Hassan, A. Ghorbani, and A. Dioszegi, "Austempered compacted graphite iron — influence of austempering temperature and time on microstructural and mechanical properties," vol. 767, p. 138434. [Online]. Available: https://www.sciencedirect.com/science/article/pii/S0921509319312201

[17] R. Elliott, *Cast iron technology*. Butterworths.

[18] J. E. Faris, "Heat treatment of compacted graphite iron."

[19] R. Ghasemi, K. Salomonsson, and A. Dioszegi, "Synergistic Effects of Austempering Variables on the Microstructure and Mechanical Properties of Low-Temperature Austenitized Compacted Graphite Irons," *Journal of Materials Engineering and Performance*, Jan. 2025. [Online]. Available: https://doi.org/10.1007/s11665-025-10636-5

[20] P. Rubin, R. Larker, E. Navara, and M.-L. Antti, "Graphite formation and dissolution in ductile irons and steels having high silicon contents: Solid-state transformations," vol. 7, no. 5, pp. 587–595. [Online]. Available: https://doi.org/10.1007/s13632-018-0478-6

[21] Y. Qiu, J. C. Pang, S. X. Li, E. N. Yang, W. Q. Fu, M. X. Liang, and Z. F. Zhang, "Influence of thermal exposure on microstructure evolution and tensile fracture behaviors of compacted graphite iron," vol. 664, pp. 75–85. [Online]. Available: https://www.sciencedirect.com/science/article/pii/S0921509316303392

[22] M. M. Jabbari Behnam, P. Davami, and N. Varahram, "Effect of cooling rate on microstructure and mechanical properties of gray cast iron," *Materials Science and Engineering: A*, vol. 528, no. 2, pp. 583–588, Dec. 2010. [Online]. Available: https://www.sciencedirect.com/science/article/pii/S0921509310011330

[23] V. Writzl, A. C. Rovani, G. Pintaude, M. S. F. Lima, W. L. Guesser, and P. C. Borges, "Scratch resistances of compacted graphite iron with plasma nitriding, laser hardening, and duplex surface treatments," vol. 143, p. 106081. [Online]. Available: https://www.sciencedirect.com/science/article/pii/S0301679X1930595X

[24] V. Writzl, M. S. F. Lima, W. L. Guesser, F. A. A. Possoli, J. C. K. das Neves, and P. C. Borges, "Influence of laser-hardening on microstructure and hardness of plasma-nitrided compacted graphite iron," vol. 144, p. 107441. [Online]. Available: https://www.sciencedirect.com/science/article/pii/S0030399221005296

[25] U. Batra, S. Ray, and S. R. Prabhakar, "Mathematical model for austenitization kinetics of ductile iron," vol. 14, no. 5, pp. 574–581. [Online]. Available: https://doi.org/10.1361/105994905X64512

[26] W. Guesser, I. Masiero, E. Melleras, and C. Cabezas, "Thermal conductivity of gray iron and compacted graphite iron used for cylinder heads," vol. 10.

[27] B. Wang, X. Han, G. C. Barber, and Y. Pan, "Wear Behavior of Austempered and Quenched and Tempered Gray Cast Irons under Similar Hardness," *Metals*, vol. 9, no. 12, p. 1329, Dec. 2019. [Online]. Available: https://www.mdpi.com/2075-4701/9/12/1329

[28] Y. G. Gurevich, "Hardenability of powder steel PK70D3 as a function of the carbon content," *Metal Science and Heat Treatment*, vol. 51, no. 3, p. 131, Oct. 2009. [Online]. Available: https://doi.org/10.1007/s11041-009-9135-7

[29] O. Idohara, Y. Hiyama, Y. Misaka, S. Takaki, and T. Tsuchiyama, "Estimation of True Hardness and Quantitative Evaluation of Auto-Tempering in As-Quenched Martensitic Steels," *ISIJ International*, vol. 64, no. 10, pp. 1599–1606, 2024.

[30] "Thermocouple | Definition & Facts | Britannica." [Online]. Available: https://www.britannica.com/technology/thermocouple

[31] "Thermal imaging cameras." [Online]. Available: https://www.micro-epsilon.com/industry-sensors/thermal-imaging-cameras/

[32] Y. Zhang, C. Zhang, L. Tan, and S. Li, "Coaxial monitoring of the fibre laser lap welding of Zn-coated steel sheets using an auxiliary illuminant," *Optics & Laser Technology*, vol. 50, pp. 167–175, Sep. 2013. [Online]. Available: https://linkinghub.elsevier.com/retrieve/pii/S0030399213000546

[33] T. A. Palmer, J. W. Elmer, and S. S. Babu, "Observations of ferrite/austenite transformations in the heat affected zone of 2205 duplex stainless steel spot welds using time resolved X-ray diffraction," *Materials Science and Engineering: A*, vol. 374, no. 1, pp. 307–321, Jun. 2004. [Online]. Available: https://www.sciencedirect.com/science/article/pii/S0921509304003053

[34] N/A, "Strong Lines of Iron (Fe)." [Online]. Available: https://physics.nist.gov/PhysRefData/Handbook/Tables/irontable2.htm

[35] A. Chakraborty, R. F. Webster, and S. Primig, "Lath martensite substructure evolution in low-carbon microalloyed steels," *Journal of Materials Science*, vol. 57, no. 22, pp. 10 359–10 378, Jun. 2022. [Online]. Available: https://doi.org/10.1007/s10853-022-07275-9

[36] S. R. Al-Sayed, A. M. Elshazli, and A. H. A. Hussein, "Laser Surface Hardening of Ni-hard White Cast Iron," *Metals*, vol. 10, no. 6, p. 795, Jun. 2020. [Online]. Available: https://www.mdpi.com/2075-4701/10/6/795

UNIVERSITY OF SKÖVDE

8 Appedix

Table 4: Experimental data from iteration 1.1

Test	Distance [mm]	Power [W]	Duration [s]	CF/RF [%]
1	676	120	0.1	100/0
2	676	500	0.1	100/0
3	676	1000	1	100/0
4	676	1000	5	100/0
5	676	2000	5	100/0
6	676	3000	5	100/0
7	676	500	5	100/0
8	676	2000	5	90/10
9	676	2000	5	80/20
10	676	2000	5	70/30
11	676	2000	5	60/40
12	676	2000	5	50/50
13	676	2000	5	40/60
14	676	2000	5	30/70
15	676	2000	5	20/80
16	676	2000	5	10/90
17	676	2000	5	0/100
18	676	3000	5	0/100
19	676	3000	10	0/100
20	676	3000	10	0/100

Table 5: Experimental data from iteration 1.2

Test	Distance [mm]	Power [W]	Duration [s]	CF/RF [%]	Emissivity
21	676	2000	10	0/100	0.3
22	676	2000	10	0/100	0.3
23	676	120	10	0/100	0.3
24	676	500	10	0/100	0.3
25	676	750	10	0/100	0.3
26	676	750	10	0/100	0.7
27	676	750	10	0/100	0.7
28	676	750	10	0/100	0.3
29	676	750	10	0/100	0.3
30	676	750	10	0/100	0.7
31	676	750	10	0/100	0.9

Table 6: Experimental data from iteration 2

Test	Distance [mm]	Power [W]	Duration [s] [1]	P0 [1]	Duration [s] [2]	P0 [2]	CF/RF [%]	Emissivity
34	676	3000	7	100%	-	0%	0/100	0.3
35	676	3000	3.2	100%	-	0%	0/100	0.3
36	676	1371	7	100%	-	0%	0/100	0.3
37	676	1500	7	100%	-	0%	0/100	0.3
38	676	2000	7	100%	-	0%	0/100	0.3
39	767	2000	7	100%	-	0%	0/100	0.3
40	767	2000	10	100%	-	0%	0/100	0.3
41	767	2000	10	50%	-	0%	0/100	0.3
42	767	2000	10	50%	5	25%	0/100	0.3
43	767	2000	10	50%	5	50%	0/100	0.3
44	767	2000	10	50%	5	50%	0/100	0.3
45	727	2000	5	75%	5	20%	0/100	0.3
46	727	2000	5	85%	15	17%	0/100	0.3

Table 7: Experimental data from iteration 3

Test	Duration [s] [1]	P0 [1]	Duration [s] [2]	P0 [2]	Duration [s] [3]	P0 [3]	C/R [%]	Emissivity
47	4	75%	1	20%	10	20%	0/100	0.3
48	4	100%	1	17%	10	17%	0/100	0.3
49	4	100%	1	17%	10	17%	0/100	0.3
50	7	100%	1	17%	10	17%	0/100	0.3
51	7	100%	1	20%	10	17%	0/100	0.3
52	7	100%	1	20%	10	17%	0/100	0.3
53	7	100%	1	20%	10	17%	0/100	0.3
54	7	75%	1	20%	10	17%	0/100	0.3
55	7	75%	1	20%	10	17%	0/100	0.7
56	7	75%	1	20%	10	17%	0/100	0.3
57	7	75%	1	20%	10	17%	0/100	0.3
58	7	85%	1	17%	10	17%	0/100	0.3
59	6	85%	1	17%	10	17%	0/100	0.3
60	6	85%	1	17%	10	17%	0/100	0.3
48b	4	75%	1	20%	10	17%	0/100	0.7
48c	4	65%	1	17%	10	17%	0/100	0.7
48d	3	65%	1	17%	10	17%	0/100	0.7
50b	2	65%	1	10%	10	10%	0/100	0.7
51b	2	65%	1	10%	10	10%	0/100	0.7
53b	2	70%	1	5%	10	5%	0/100	0.7
53c	2	65%	1	3%	10	5%	0/100	0.7
54b	2	60%	1	5%	10	5%	0/100	0.7
56b	2	62%	1	4%	10	5%	0/100	0.7
58b	2	62%	1	4%	10	5%	0/100	0.7
58c	2	63%	1	5%	10	5%	0/100	0.7

UNIVERSITY OF SKÖVDE

Table 8: Experimental data from iteration 4

Test	Power [W]	Duration [s] [1]	P0 [1]	Duration [s] [2]	P0 [2]	Duration [s] [3]	P0 [3]
61	2000	5	63%	1	5%	-	-
62	3000	10	100%	1	10%	-	-
63	4000	10	100%	-	-	-	-
64	4000	10	80%	-	-	-	-
65	4000	10	80%	-	-	-	-
66	3000	10	100%	-	-	10	15%
67	4000	10	80%	0.1	15%	10	15%
68	4000	10	90%	0.1	45%	10	20%
69	4000	10	90%	5	70%	5	15%
70	4000	10	85%	5	60%	5	15%
71	5000	10	70%	5	5%	5	5%
72	5000	10	70%	5	20%	5	10%
73	5000	10	70%	0.1	20%	10	15%
74	5000	10	80%	0.1	20%	10	15%
75	-	-	-	-	-	-	-
76	5000	10	75%	0.1	20%	60	15%
77	5000	10	78%	0.1	30%	60	13%
78	5000	10	78%	0.1	30%	60	13%
79	5000	10	78%	-	-	60	13%
80	5000	10	77%	-	-	60	15%
81	5000	10	80%	-	-	60	13%
82	5000	10	83%	0.1	30%	60	14%
83	5000	10	85%	-	-	60	12.5%
84	5000	10	87%	-	-	60	12%
85	5000	8	87%	2	50%	60	12%
86	5000	9	87%	1	50%	60	12%
87	5000	9.5	87%	0.5	25%	60	12%
88	5000	9	87%	1	15%	60	12%
89	5000	10	87%	-	-	300	˜12%
90	5000	10	85%	-	-	300	˜12%
91	5000	10	85%	-	-	180	˜12%
92	5000	10	84%	-	-	180	˜12%
93	5000	10	83%	-	-	180	˜12%
94	5000	10	84%	-	-	180	˜12%
95	5000	10	84%	-	-	180	˜12%
96	5000	10	85%	-	-	180	˜12%
97	5000	10	85%	-	-	180	˜12%
98	5000	10	85%	-	-	180	˜12%
99	5000	10	85%	-	-	180	˜12%
100	5000	10	85%	-	-	180	˜12%
101	5000	10	85%	-	-	60	˜12%
102	5000	10	85%	-	-	120	˜12%
103	5000	10	85%	-	-	120	˜12%
104	5000	10	85%	-	-	120	˜12%
105	5000	10	85%	-	-	120	˜12%
106	5000	10	85%	-	-	120	˜12%

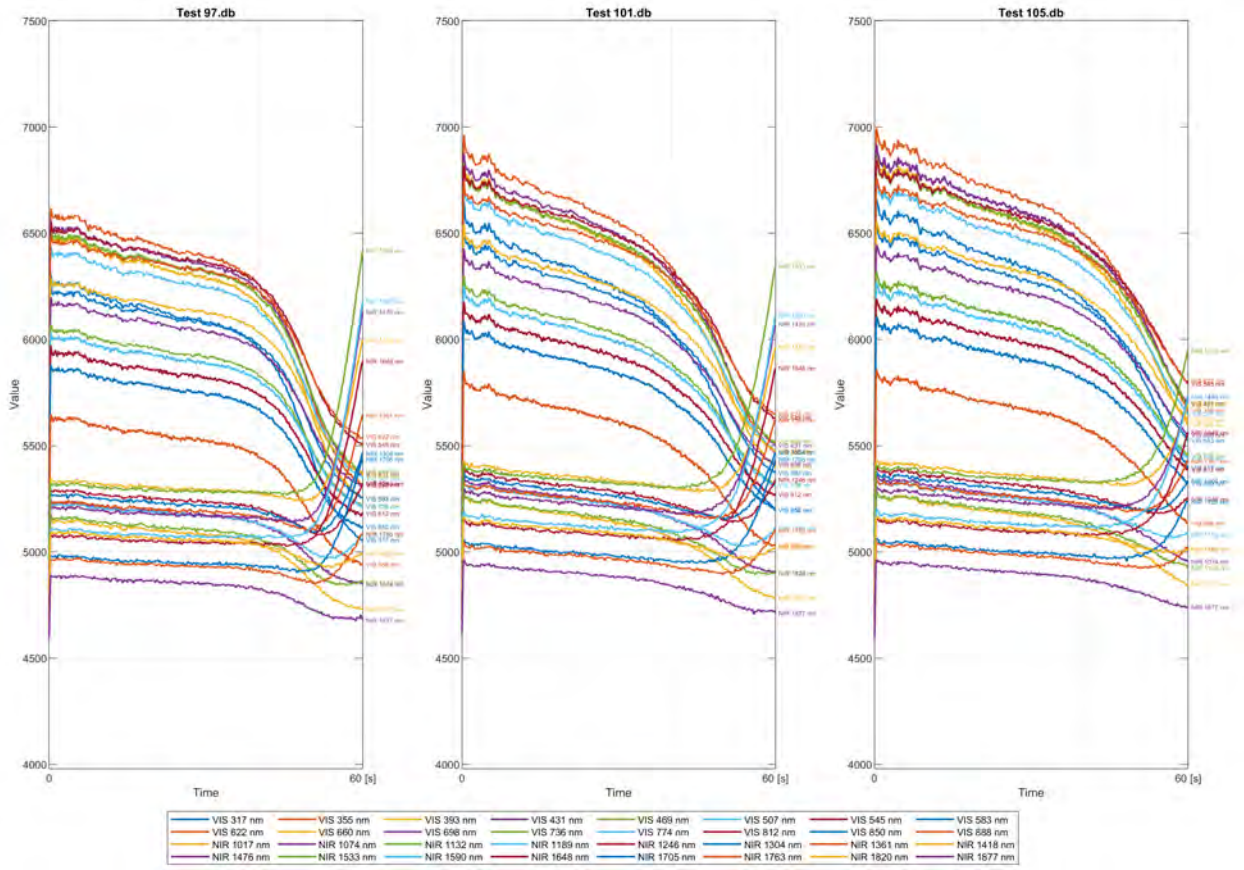

Figure 41: Comparison of photodiode signal by tests in iteration 4.

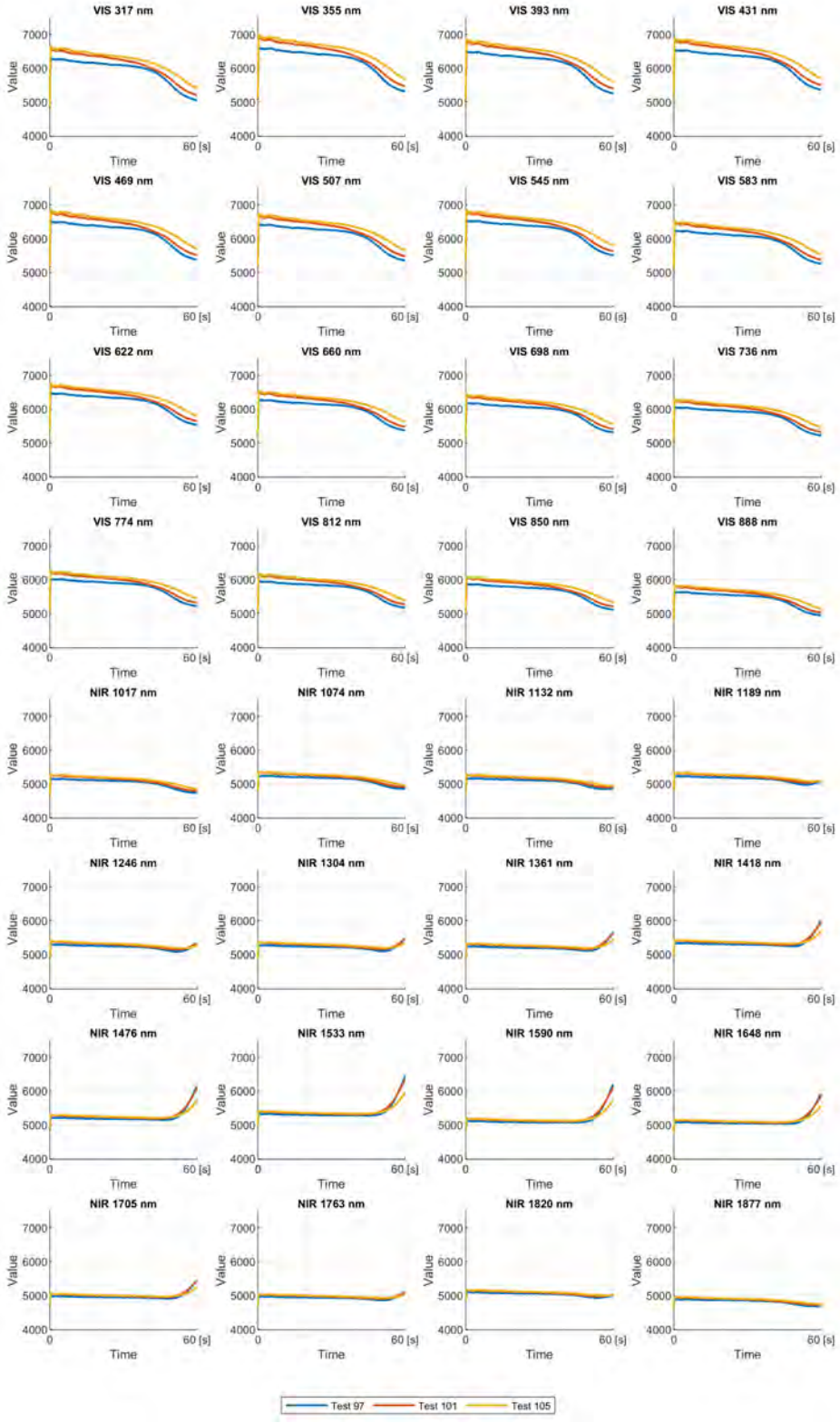

Figure 42: Comparison of photodiode signal by wavelength in iteration 4.

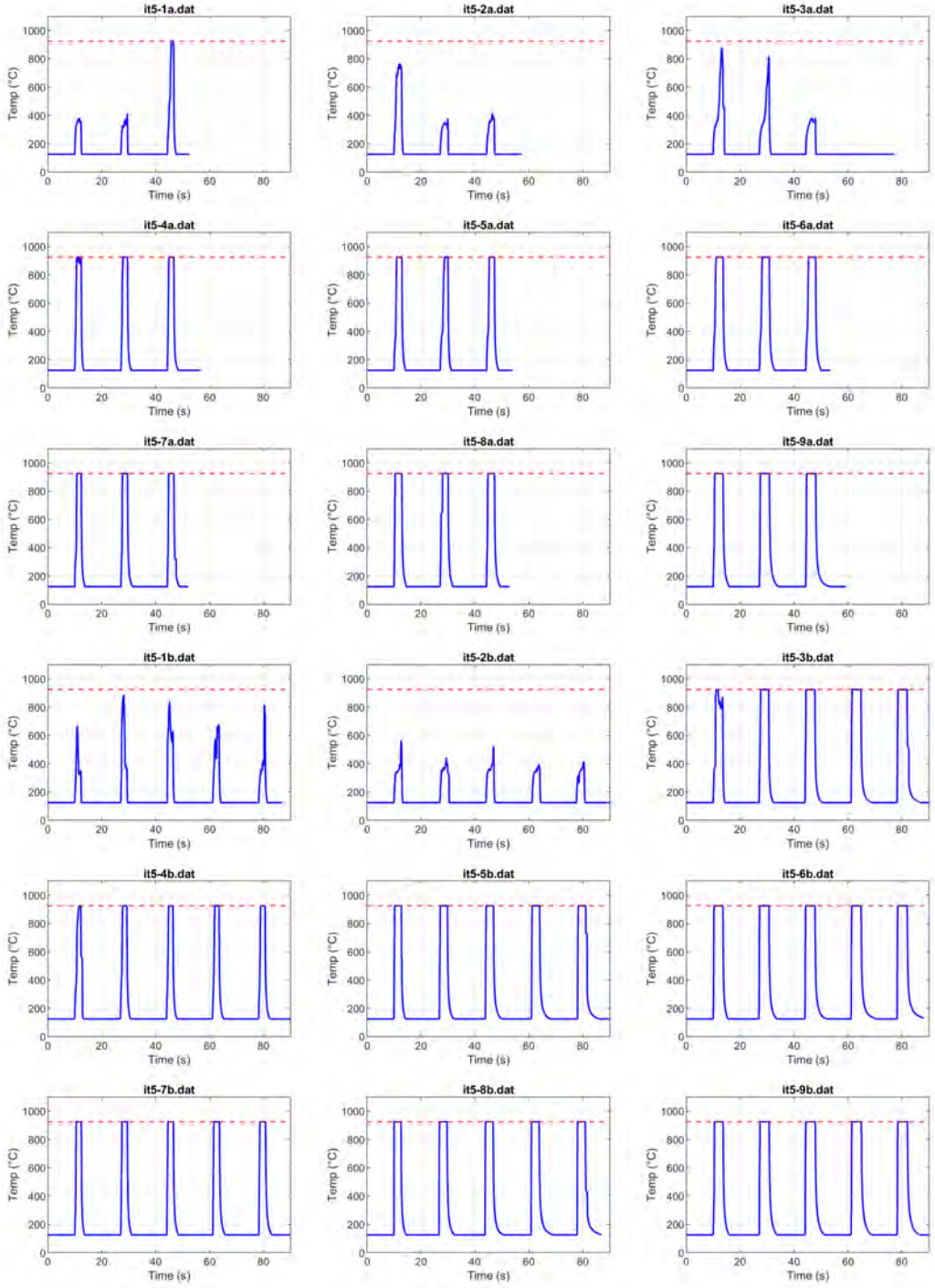

Figure 43: Thermal imager data from the 18 tests in iteration 5.

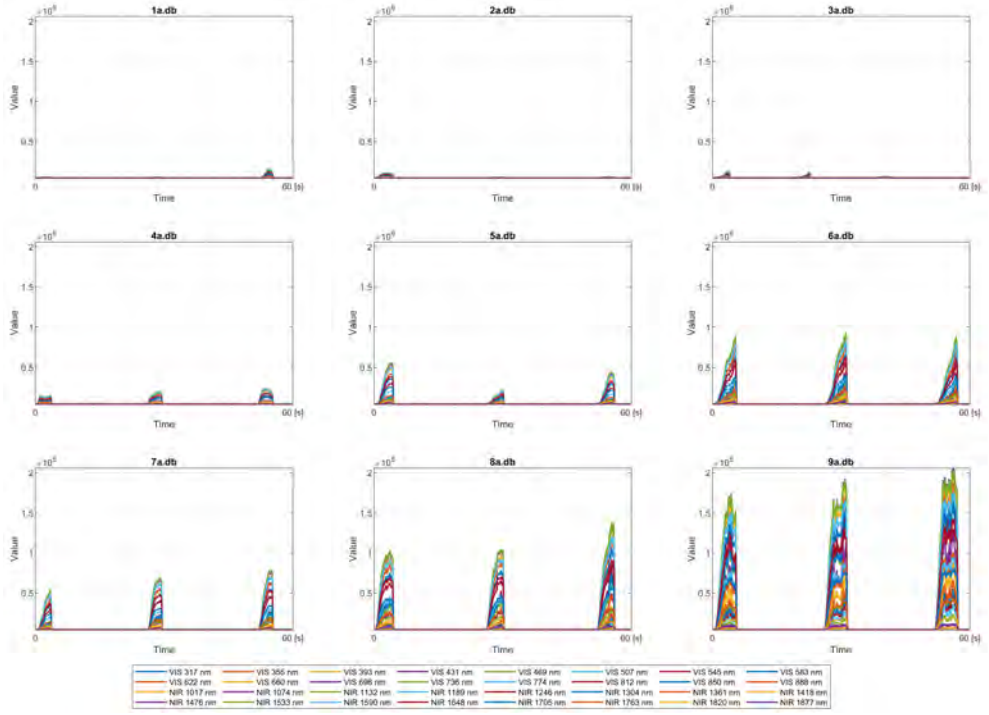

Figure 44: Comparison of photodiode signal by tests of 3 lines in iteration 5.

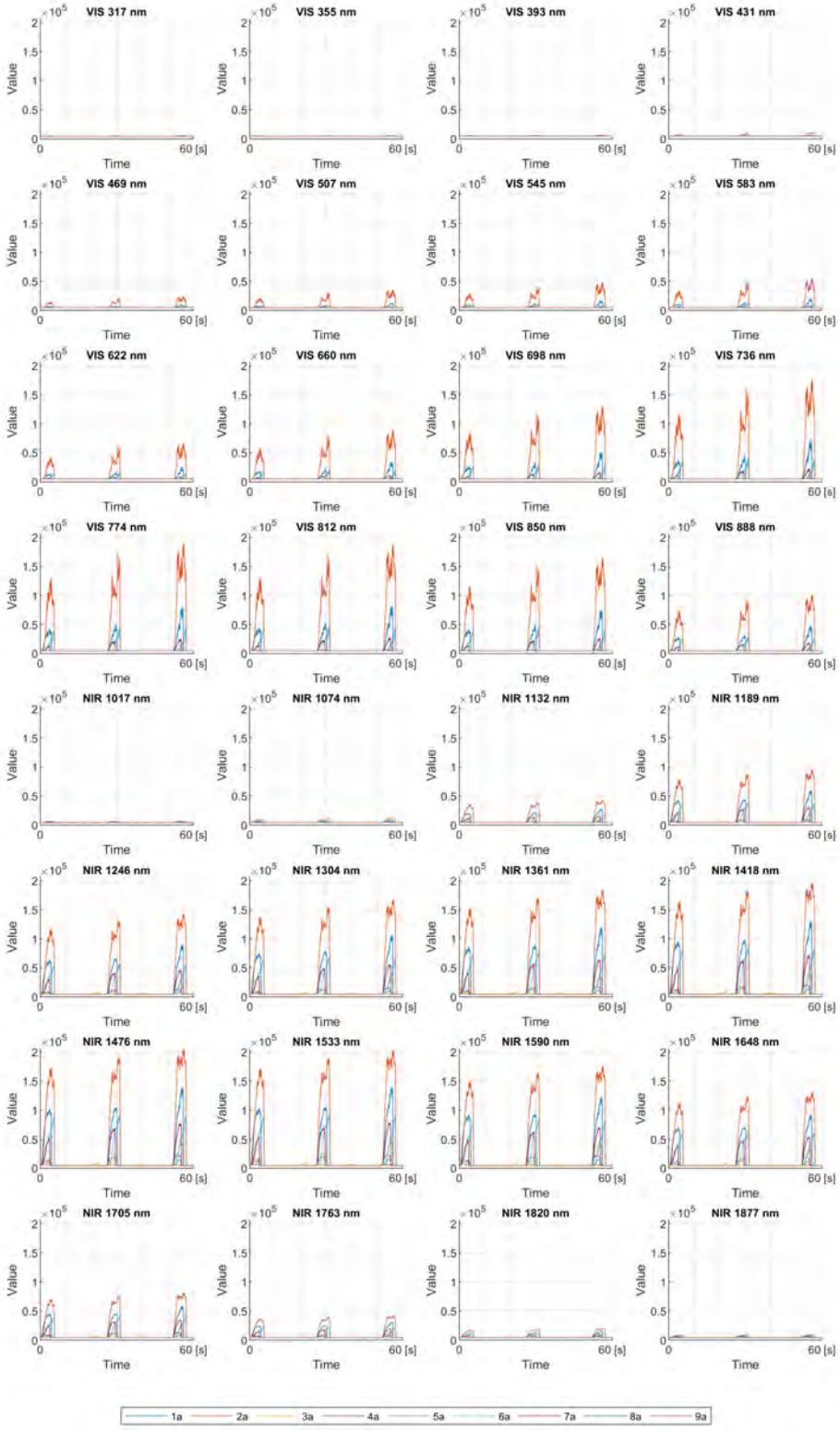

Figure 45: Comparison of photodiode signal by wavelength of 3 lines in iteration 5.

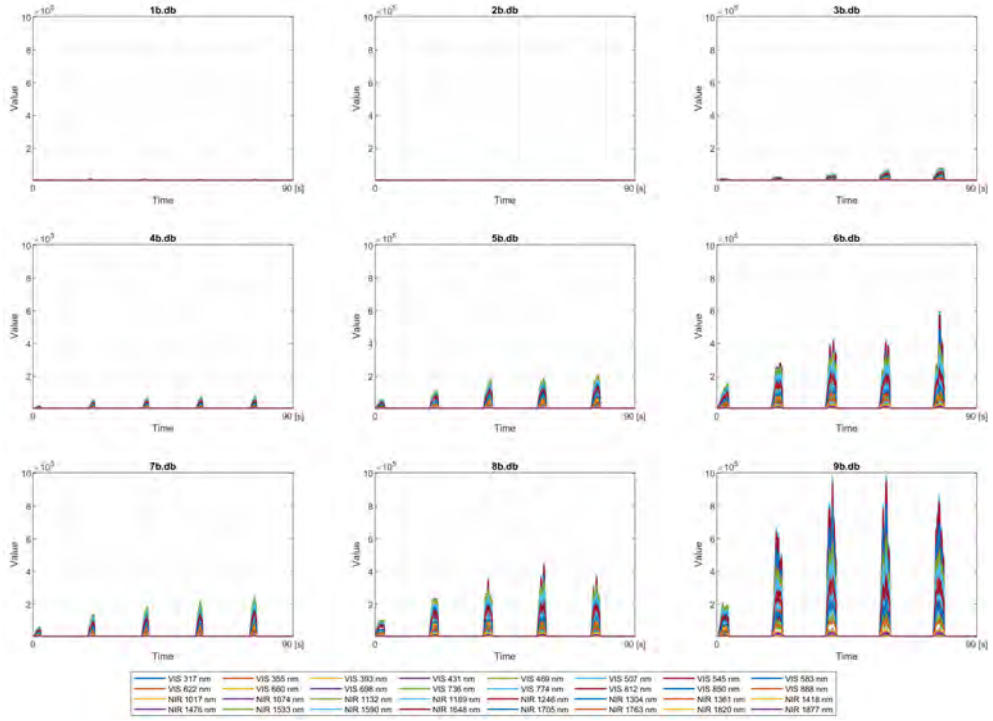

Figure 46: Comparison of photodiode signal by tests of 5 lines in iteration 5.

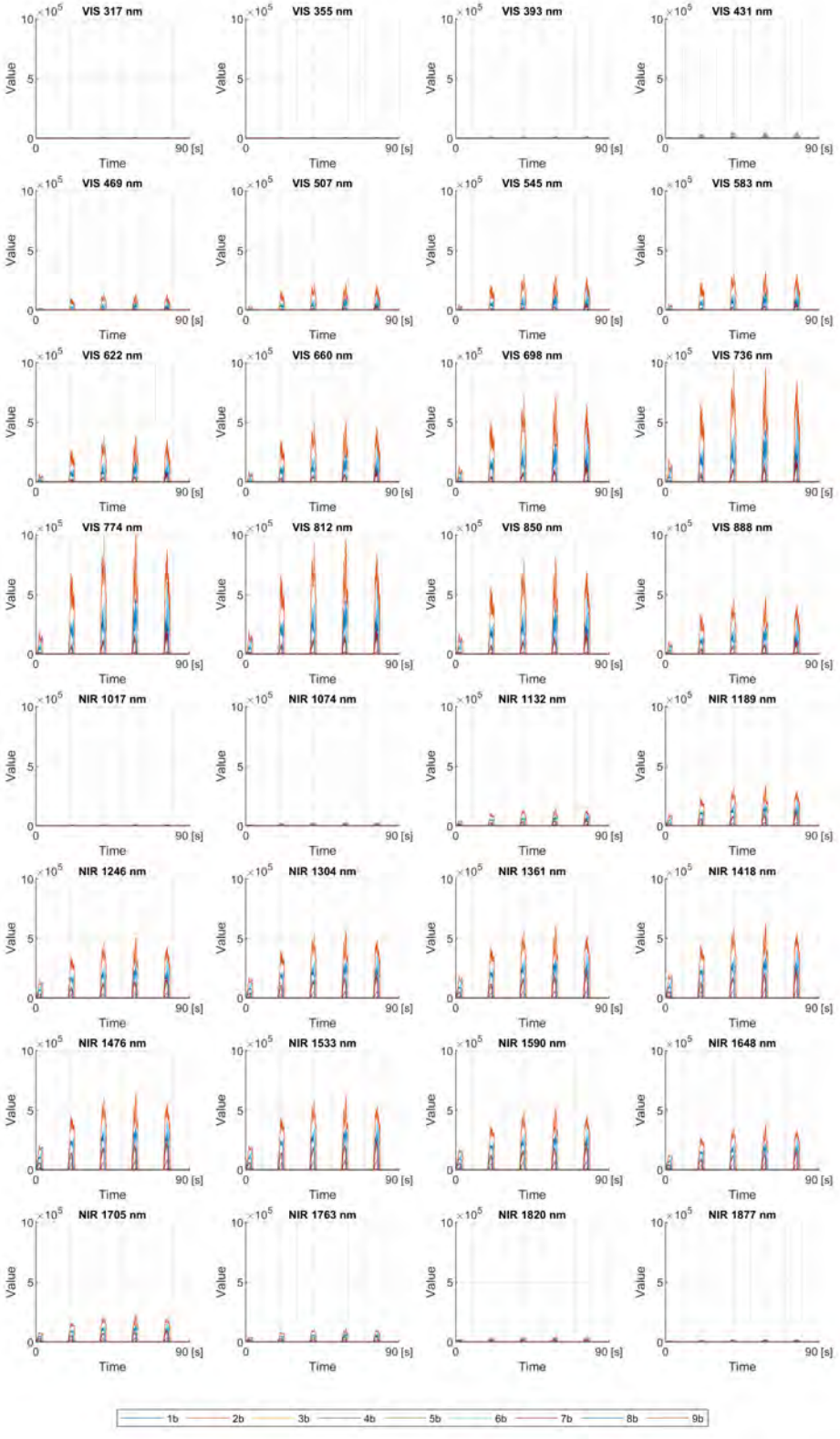

Figure 47: Comparison of photodiode signal by wavelength of 5 lines in iteration 5.

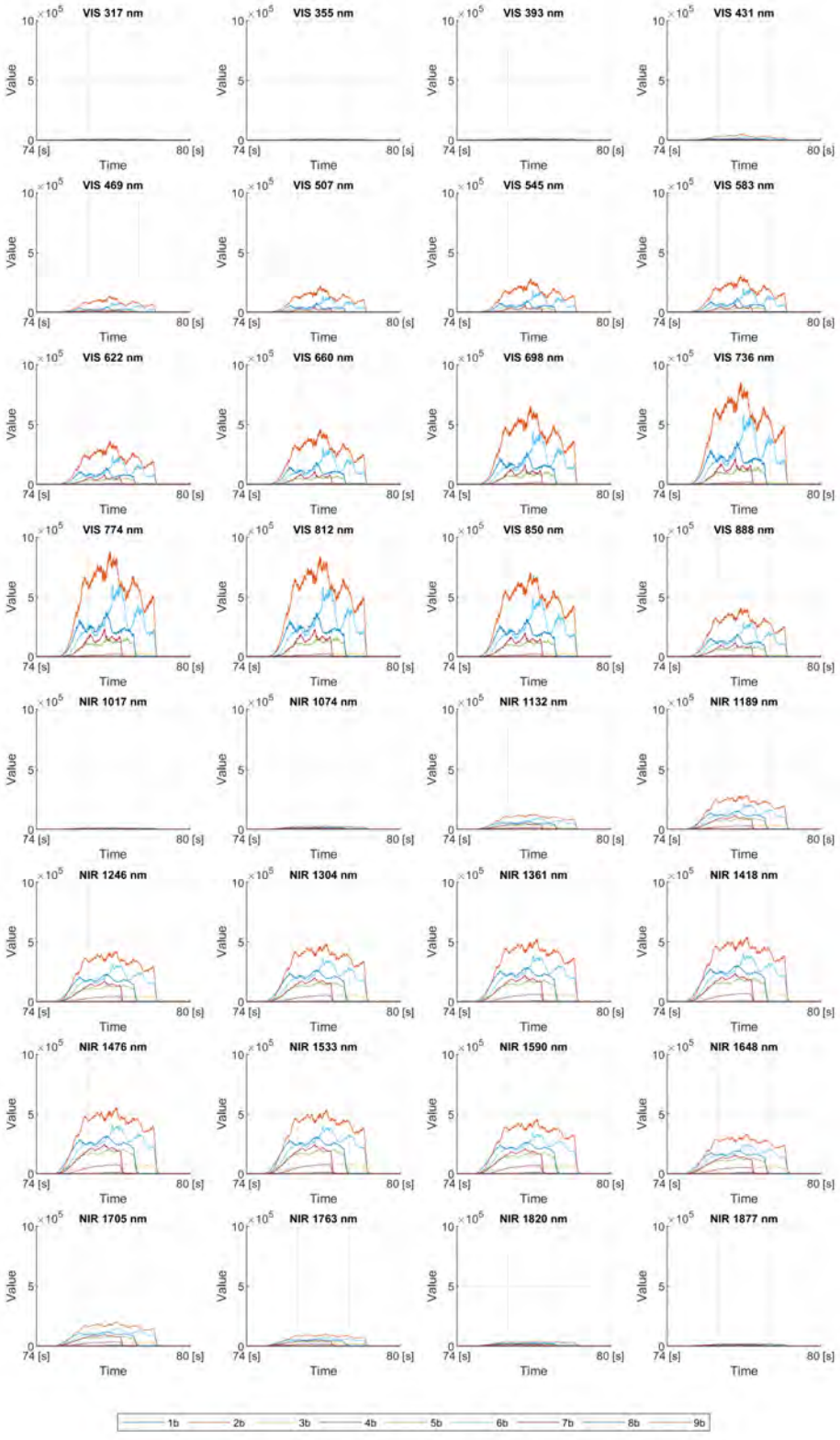

Figure 48: Comparison example of photodiode signal by wavelength from third line of 5 lines in iteration 5.